DRIFT CAPACITY OF REINFORCED CONCRETE COLUMNS SUBJECTED TO DISPLACEMENT REVERSALS

A Thesis

Submitted to the Faculty

of

Purdue University

by

Santiago Pujol

In Partial Fulfillment of the

Requirements for the Degree

of

Doctor of Philosophy

August 2002

ACKNOWLEDGMENTS

The writer would like to express his deepest gratitude for the help, guidance and support provided by his mentors, Professors Mete A. Sozen and Julio A Ramirez.

Special recognition is given to Professors C. D. Sutton, and T. Farris for being part of the advisory committee.

The assistance of Harry Tidrick, Linda Vail, Tracy Mavity, Amber Vibbert, and the personnel of Purdue University Central Machine Shop is greatly appreciated.

Data collection would have not been possible without the help of Zachary Zolvinski, Keith Law, Lister Carbon, Juan Pablo García, James Reisert, Kyle Fisher, Anita Jacobson, and Jennifer Ridd. Their patience and dedication was invaluable.

Finally, the writer would like to thank his parents, Pedro and Martha, his brother, Andrés, his sister, Martha C., and his friends, Gerardo Aguilar, Jhon Paul Smith, Lisa Samples, Jon Jonsson, Brian Malone, Michael Appelhans, Koray Tureyen, Yeliz Firat, and Isabel Castelao, for their encouragement and help.

TABLE OF CONTENTS

	Page
LIST OF TABLES	vi
LIST OF FIGURES	vii
ABSTRACT	xxiv
1 INTRODUCTION	1
1.1 Background	1
1.2 Previous Investigations	1
1.3 Objective and Scope	3
1.4 Preliminary Criterion for Classification of Available Data	4
2 EXPERIMENTS	8
2.1 Introduction	8
2.2 Observed Shear-Drift Ratio Response	9
2.2.1 First Displacement Cycle	10
2.2.2 Subsequent Cycles	10
2.3 Failure	11
2.4 Stiffness vs. Number of Cycles	12
2.5 Transverse Deformations	13
2.6 Longitudinal Reinforcement Unit Strains	14
2.7 Hoop Unit Strains	15
2.8 Rotation	15
2.9 Internal Forces	16
2.10 Comparisons: Effect of Independent Variables	18
2.10.1 Hoop Spacing	19
2.10.2 Axial Load	20
2.10.3 Displacement History	21

	Page
3 DISPLACEMENT COMPONENTS	23
3.1 Introduction	23
3.2 Calculation of Displacement Components	23
3.3 Displacement Components vs. Number of Cycles	26
3.4 Theoretical Displacement Components	27
4 TWO MODELS	32
4.1 Introduction	32
4.2 Transverse Deformations	32
4.3 Model A	33
4.4 Model B	35
4.5 Results	38
4.6 Comparison with Data from Previous Experiments	38
4.7 Number of Cycles for Recorded Ground Motions	40
5 SUMMARY AND CONCLUSIONS	45
5.1 Summary	45
5.1.1 Objective and Scope	45
5.1.2 Previous Investigations	46
5.1.3 Experimental Program	46
5.1.3.1 Test Specimens	46
5.1.3.2 Response	47
5.1.3.3 Effect of Independent Variables	47
5.1.4 Displacement Components	48
5.1.5 Models	48
5.1.6 Number of Cycles for Recorded Ground Motions	48
5.2 Conclusions	49
LIST OF REFERENCES	50
VOLUME II	
TABLES	53
EICLIDEC	60

	Page
APPENDIX	
A.1 Introduction	271
A.2 Materials	271
A.2.1 Concrete	271
A.2.2 Reinforcement	272
A.3 Description of Test Assemblies	273
A.3.1 Dimensions	274
A.3.2 Reinforcement Details	274
A.3.3 Casting and Curing	275
A.4 Test Procedure	275
A.4.1 Loading Frame	275
A.4.2 Measurements	277
A.4.3 Instrumentation	278
A.4.4 Testing Sequence	280
VITA	310

LIST OF TABLES

Table		Page
1.4-1	Previous Experimental Data.	53
2.1-1	Experimental Program.	54
2.2.2-1	Observed Shear-Drift Ratio Response.	54
2.4-1	Experimental Results	55
3.4-1	Indentation Measured at the Level of the Reinforcement Under Compression During First Yield.	56
4.3-1	Model A, Parameters and Results.	
4.3-2	Model B, Results.	57
4.7-1	Number of Large Displacement Peaks for an Idealized 10-Story Regular Reinforced Concrete Frame Subjected to Base Accelerations Modeled after Recorded Ground Motions Scaled to 0.4g Peak Ground	
	Acceleration.	58
4.7-2	Number of Large Displacement Peaks for an Idealized 20-Story Regular Reinforced Concrete Frame Subjected to Base Accelerations Modeled after Recorded Ground Motions Scaled to 0.4g Peak Ground Acceleration.	58
4.7-3	Number of Large Displacement Peaks for an Idealized 30-Story Regular Reinforced Concrete Frame Subjected to Base Accelerations Modeled after Recorded Ground Motions Scaled to 0.4g Peak Ground Acceleration.	59
Appendi	x Table	
A.2.1-1	Mix Proportions and Concrete Batch Designations	282
A.2.1-2	Measured Concrete Properties.	283
A.2.2-1	Measured Reinforcement Properties.	284

LIST OF FIGURES

Figure	Page
1.4-1	Coulomb's Failure Criterion
1.4-2	Maximum Drift Ratio vs. Parameter k_1
1.4-3	Specimens Tested by Ohue et al. (1985) and Ono et al. (1989),
	Displacement History and Geometry
1.4-4	Specimens Tested by Saatcioglu and Ozcebe (1989), and Sakai et al.
	(1990), Displacement History and Geometry
1.4-5	Specimens Tested by Wight (1973), and Xiao and Martirossyan (1998),
	Displacement History and Geometry
2.1-1	Description of Test Assembly
2.1-2	Whittemore Gage Measurements
2.2-1	Shear vs. Drift Ratio, Specimen 10-2-3 North
2.2-2	Shear vs. Drift Ratio, Specimen 10-2-3 South
2.2-3	Shear vs. Drift Ratio, Specimen 10-3-11/2 North
2.2-4	Shear vs. Drift Ratio, Specimen 10-3-1½ South
2.2-5	Shear vs. Drift Ratio, Specimen 10-3-3 North
2.2-6	Shear vs. Drift Ratio, Specimen 10-3-3 South
2.2-7	Shear vs. Drift Ratio, Specimen 10-3-21/4 North
2.2-8	Shear vs. Drift Ratio, Specimen 10-3-21/4 South
2.2-9	Shear vs. Drift Ratio, Specimen 20-3-1½ North70
2.2-10	Shear vs. Drift Ratio, Specimen 20-3-1½ South70
2.2-11	Shear vs. Drift Ratio, Specimen 20-3-3 North
2.2-12	Shear vs. Drift Ratio, Specimen 20-3-3 South
2.2-13	Shear vs. Drift Ratio, Specimen 10-2-21/4 North
2.2-14	Shear vs. Drift Ratio, Specimen 10-2-21/4 South

Figure	Page
2.2-15	Shear vs. Drift Ratio, Specimen 10-1-2 ¹ / ₄ North
2.2-16	Shear vs. Drift Ratio, Specimen 10-1-2 ¹ / ₄ South
2.2.1-1	Concrete Spalling, Specimen 10-3-3 North, 1% Drift Ratio, Cycle 174
2.2.1-2	Concrete Spalling, Specimen 20-3-3 South, 1% Drift Ratio, Cycle 174
2.2.1-3	Concrete Spalling During First Cycle, Specimen 10-3-21/4 North
2.2.1-4	Cracking Pattern, First Load Cycle, Specimens 10-2-376
2.2.1-5	Cracking Pattern, First Load Cycle, Specimens 10-3-1 ½77
2.2.1-6	Cracking Pattern, First Load Cycle, Specimens 10-3-378
2.2.1-7	Cracking Pattern, First Load Cycle, Specimens 10-3-2 ¹ / ₄
2.2.1-8	Cracking Pattern, First Load Cycle, Specimens 20-3-1½80
2.2.1-9	Cracking Pattern, First Load Cycle, Specimens 20-3-3
2.2.1-10	Cracking Pattern, First Load Cycle, Specimens 10-2-21/4
2.2.1-11	Cracking Pattern, First Load Cycle, Specimens 10-1-21/4
2.2.2-1	Specimens 10-2-3 After Cycle 7
2.2.2-2	Specimens 10-2-3 After Cycle 11
2.2.2-3	Specimens 10-2-3 During Cycle 14
2.2.2-4	Specimens 10-3-1½ During Cycle 7
2.2.2-5	Specimens 10-3-1½ During Cycle 14
2.2.2-6	Specimens 10-3-11/2 After Cycle 16
2.2.2-7	Specimens 10-3-1½ During Cycle 18
2.2.2-8	Specimens 10-3-3 During Cycle 6
2.2.2-9	Specimens 10-3-3 During Cycle 9
2.2.2-10	Specimens 10-3-2 ¹ / ₄ During Cycle 7
2.2.2-11	Specimens 10-3-2 ¹ / ₄ During Cycle 14
2.2.2-12	Specimens 10-3-21/4 After Cycle 19
2.2.2-13	Specimens 20-3-1½ During Cycle 7
2.2.2-14	Buckling of Longitudinal Reinforcement, Specimen 20-3-1½ North 92
2.2.2-15	Specimens 20-3-1½ During Cycle 16. 92
2.2.2-16	Specimens 20-3-3 During Cycle 7

Figure		Page
2.2.2-17	Specimens 20-3-3 During Cycle 9.	93
2.2.2-18	Specimens 10-2-2 ¹ / ₄ During Cycle 7.	94
2.2.2-19	Specimens 10-2-2 ¹ / ₄ During Cycle 14.	94
2.2.2-20	Specimens 10-2-2 ¹ / ₄ During Cycle 19.	95
2.2.2-21	Specimens 10-2-2 ¹ / ₄ During Cycle 23.	95
2.2.2-22	Specimens 10-1-2 ¹ / ₄ During Cycle 7.	96
2.2.2-23	Specimens 10-1-2 ¹ / ₄ During Cycle 14.	96
2.2.2-24	Specimens 10-1-2 ¹ / ₄ During Cycle 21.	97
2.2.2-25	Specimens 10-1-2 ¹ / ₄ During Cycle 27.	97
2.3-1	Specimen 10-2-3 North at the End of the Test.	98
2.3-2	Specimen 10-3-11/2 South at the End of the Test.	98
2.3-3	Specimen 10-3-3 North at the End of the Test.	99
2.3-4	Specimen 10-3-2 North at the End of the Test.	99
2.3-5	Specimen 20-3-3 South at the End of the Test.	. 100
2.3-6	Specimen 10-2-21/4 North at the End of the Test.	. 100
2.3-7	Specimen 10-1-21/4 South at the End of the Test.	. 101
2.3-8	Specimens10-3-11/2 After Removal of Loose Concrete.	. 102
2.3-9	Detail of Specimen10-3-11/2 South After Removal of Loose Concrete	. 102
2.3-10	Specimens 10-3-3 After Removal of Loose Concrete.	. 103
2.3-11	Detail of Specimen 10-3-3 North After Removal of Loose Concrete	. 103
2.3-12	Specimens 10-3-21/4 After Removal of Loose Concrete.	. 104
2.3-13	Detail of Specimen 10-3-21/4 North After Removal of Loose Concrete	. 104
2.3-14	Specimens 20-3-3 After Removal of Loose Concrete.	. 105
2.3-15	Detail of Specimen 20-3-3 South After Removal of Loose Concrete	. 105
2.3-16	Specimens 10-2-21/4 After Removal of Loose Concrete.	. 106
2.3-17	Detail of Specimen 10-2-21/4 North After Removal of Loose Concrete	. 106
2.3-18	Specimens 10-1-2 ¹ / ₄ After Removal of Loose Concrete.	. 107
2.3-19	Detail of Specimen 10-1-21/4 South After Removal of Loose Concrete	. 107
2.4-1	Variation of Stiffness with Number of Cycles, Specimen 10-2-3 North	. 108

Figure	Page
2.4-2	Variation of Stiffness with Number of Cycles, Specimen 10-3-11/2
	South
2.4-3	Variation of Stiffness with Number of Cycles, Specimen 10-3-3 North 109
2.4-4	Variation of Stiffness with Number of Cycles, Specimen 10-3-2 1/4
	North
2.4-5	Variation of Stiffness with Number of Cycles, Specimen 20-3-11/2
	North
2.4-6	Variation of Stiffness with Number of Cycles, Specimen 20-3-3 South 110
2.4-7	Variation of Stiffness with Number of Cycles, Specimen 10-2-21/4
	North
2.4-8	Variation of Stiffness with Number of Cycles, Specimen 10-1-21/4
	South
2.5-1	Transverse Deformations, Specimen 10-2-3 North
2.5-2	Transverse Deformations, Specimen 10-2-3 South
2.5-3	Transverse Deformations, Specimen 10-3-1½ North
2.5-4	Transverse Deformations, Specimen 10-3-1½ South
2.5-5	Transverse Deformations, Specimen 10-3-3 North
2.5-6	Transverse Deformations, Specimen 10-3-3 South
2.5-7	Transverse Deformations, Specimen 10-3-2 ¹ / ₄ North
2.5-8	Transverse Deformations, Specimen 10-3-2 ¹ / ₄ South
2.5-9	Transverse Deformations, Specimen 20-3-1½ North
2.5-10	Transverse Deformations, Specimen 20-3-1½ South
2.5-11	Transverse Deformations, Specimen 20-3-3 North
2.5-12	Transverse Deformations, Specimen 20-3-3 South
2.5-13	Transverse Deformations, Specimen 10-2-2 ¹ / ₄ North
2.5-14	Transverse Deformations, Specimen 10-2-2 ¹ / ₄ South
2.5-15	Transverse Deformations, Specimen 10-1-2 ¹ / ₄ North
2.5-16	Transverse Deformations, Specimen 10-1-2 ¹ / ₄ South

Figure		Page
2.5-17	Cycle Number at 20% Stiffness loss vs. Cycle Number at 0.25-in.	
	Measured Transverse Deformation.	120
2.5-18	Transverse Deformations vs. Inclined Crack Width, Specimens 10-2-3	121
2.5-19	Transverse Deformations vs. Inclined Crack Width, Specimens 10-3-	
	1½	121
2.5-20	Transverse Deformations vs. Inclined Crack Width, Specimens 10-3-3	122
2.5-21	Transverse Deformations vs. Inclined Crack Width, Specimens 10-3-	
	21/4	122
2.5-22	Transverse Deformations vs. Inclined Crack Width, Specimens 20-3-	
	1½	123
2.5-23	Transverse Deformations vs. Inclined Crack Width, Specimens 20-3-3	123
2.5-24	Transverse Deformations vs. Inclined Crack Width, Specimens 10-2-	
	21/4	124
2.5-25	Transverse Deformations vs. Inclined Crack Width, Specimens 10-1-	
	21/4	124
2.6-1	Longitudinal Reinforcement Unit Strains vs. Drift Ratio, Specimens 10-	
	2-3	125
2.6-2	Longitudinal Reinforcement Unit Strains vs. Drift Ratio, Specimens 10-	
	2-3	126
2.6-3	Longitudinal Reinforcement Unit Strains vs. Drift Ratio, Specimens 10-	
	3-1½	127
2.6-4	Longitudinal Reinforcement Unit Strains vs. Drift Ratio, Specimens 10-	
	3-1½	128
2.6-5	Longitudinal Reinforcement Unit Strains vs. Drift Ratio, Specimens 10-	
	3-3	129
2.6-6	Longitudinal Reinforcement Unit Strains vs. Drift Ratio, Specimens 10-	
	3-3	130
2.6-7	Longitudinal Reinforcement Unit Strains vs. Drift Ratio, Specimens 10-	
	3-21/4	131

Figure		Page
2.6-8	Longitudinal Reinforcement Unit Strains vs. Drift Ratio, Specimens 10-	
	3-21/4	132
2.6-9	Longitudinal Reinforcement Unit Strains vs. Drift Ratio, Specimens 20-	
	3-1½	133
2.6-10	Longitudinal Reinforcement Unit Strains vs. Drift Ratio, Specimens 20-	
	3-1½	134
2.6-11	Longitudinal Reinforcement Unit Strains vs. Drift Ratio vs. Drift Ratio,	
	Specimens 20-3-3	135
2.6-12	Longitudinal Reinforcement Unit Strains vs. Drift Ratio vs. Drift Ratio,	
	Specimens 20-3-3	136
2.6-13	Longitudinal Reinforcement Unit Strains vs. Drift Ratio, Specimens 10-	
	2-21/4	137
2.6-14	Longitudinal Reinforcement Unit Strains vs. Drift Ratio, Specimens 10-	
	2-21/4	138
2.6-15	Longitudinal Reinforcement Unit Strains vs. Drift Ratio, Specimens 10-	
	1-21/4	139
2.6-16	Longitudinal Reinforcement Unit Strains vs. Drift Ratio, Specimens 10-	
	1-21/4	140
2.7-1	Transverse Reinforcement Unit Strains vs. Drift Ratio, Specimens 10-2-	
	3	141
2.7-2	Transverse Reinforcement Unit Strains vs. Drift Ratio, Specimens 10-2-	
	3	142
2.7-3	Transverse Reinforcement Unit Strains vs. Drift Ratio, Specimens 10-2-	
	3	143
2.7-4	Transverse Reinforcement Unit Strains vs. Drift Ratio, Specimens 10-2-	
	3	144
2.7-5	Transverse Reinforcement Unit Strains vs. Drift Ratio, Specimens 10-3-	
	$1\frac{1}{2}$	145

Figure		Page
2.7-6	Transverse Reinforcement Unit Strains vs. Drift Ratio, Specimens 10-3-	116
	1½	140
2.7-7	Transverse Reinforcement Unit Strains vs. Drift Ratio, Specimens 10-3-1½	147
27.0		14/
2.7-8	Transverse Reinforcement Unit Strains vs. Drift Ratio, Specimens 10-3-1½.	148
2.7-9	Transverse Reinforcement Unit Strains vs. Drift Ratio, Specimens 10-3-	
2.1-7	3	149
2.7-10	Transverse Reinforcement Unit Strains vs. Drift Ratio, Specimens 10-3-	
2.7 10	3	150
2.7-11	Transverse Reinforcement Unit Strains vs. Drift Ratio, Specimens 10-3-	
	3	151
0.7.10		131
2.7-12	Transverse Reinforcement Unit Strains vs. Drift Ratio, Specimens10-3-	
	3	152
2.7-13	Transverse Reinforcement Unit Strains vs. Drift Ratio, Specimens 10-3-	
	21/4	153
2.7-14	Transverse Reinforcement Unit Strains vs. Drift Ratio, Specimens 10-3-	
	21/4	154
2.7-15	Transverse Reinforcement Unit Strains vs. Drift Ratio, Specimens 10-3-	
21, 10	2½	155
2.7-16	Transverse Reinforcement Unit Strains vs. Drift Ratio, Specimens 10-3-	
2.7-10		156
	2½	156
2.7-17	Transverse Reinforcement Unit Strains vs. Drift Ratio, Specimens 20-3-	
	1½	157
2.7-18	Transverse Reinforcement Unit Strains vs. Drift Ratio, Specimens 20-3-	
	1½	158
2.7-19	Transverse Reinforcement Unit Strains vs. Drift Ratio, Specimens 20-3-	
	1½	159

Figure	Page
2.7-20	Transverse Reinforcement Unit Strains vs. Drift Ratio, Specimens 20-3-
	1½
2.7-21	Transverse Reinforcement Unit Strains vs. Drift Ratio, Specimens 20-3-
	3161
2.7-22	Transverse Reinforcement Unit Strains vs. Drift Ratio, Specimens 20-3-
	3162
2.7-23	Transverse Reinforcement Unit Strains vs. Drift Ratio, Specimens 20-3-
	3163
2.7-24	Transverse Reinforcement Unit Strains vs. Drift Ratio, Specimens 20-3-
	3164
2.7-25	Transverse Reinforcement Unit Strains vs. Drift Ratio, Specimens 10-2-
	21/4
2.7-26	Transverse Reinforcement Unit Strains vs. Drift Ratio, Specimens 10-2-
	21/4
2.7-27	Transverse Reinforcement Unit Strains vs. Drift Ratio, Specimens 10-2-
	21/4
2.7-28	Transverse Reinforcement Unit Strains vs. Drift Ratio, Specimens 10-2-
	21/4
2.7-29	Transverse Reinforcement Unit Strains vs. Drift Ratio, Specimens 10-1-
	21/4
2.7-30	Transverse Reinforcement Unit Strains vs. Drift Ratio, Specimens 10-1-
	21/4
2.7-31	Transverse Reinforcement Unit Strains vs. Drift Ratio, Specimens 10-1-
	21/4
2.7-32	Transverse Reinforcement Unit Strains vs. Drift Ratio, Specimens 10-1-
	21/4
2.8-1	Rotation vs. Drift Ratio, Specimen 10-2-3 North
2.8-3	Rotation vs. Drift Ratio, Specimen 10-3-1½ North
2.8-4	Rotation vs. Drift Ratio, Specimen 10-3-1½ South

Figure	Page
2.8-5	Rotation vs. Drift Ratio, Specimen 10-3-3 North
2.8-6	Rotation vs. Drift Ratio, Specimen 10-3-3 South
2.8-7	Rotation vs. Drift Ratio, Specimen 10-3-21/4 North
2.8-8	Rotation vs. Drift Ratio, Specimen 10-3-21/4 South
2.8-9	Rotation vs. Drift Ratio, Specimen 20-3-11/2 North
2.8-10	Rotation vs. Drift Ratio, Specimen 20-3-11/2 South
2.8-11	Rotation vs. Drift Ratio, Specimen 20-3-3 North
2.8-12	Rotation vs. Drift Ratio, Specimen 20-3-3 South
2.8-13	Rotation vs. Drift Ratio, Specimen 10-2-21/4 North
2.8-14	Rotation vs. Drift Ratio, Specimen 10-2-21/4 South
2.8-15	Rotation vs. Drift Ratio, Specimen 10-1-21/4 North
2.8-16	Rotation vs. Drift Ratio, Specimen 10-1-21/4 South
2.8-17	Transverse Reinforcement Unit Strains vs. Rotation, Specimens 10-2-3 181
2.8-18	Transverse Reinforcement Unit Strains vs. Rotation, Specimens 10-2-3 182
2.8-19	Transverse Reinforcement Unit Strains vs. Rotation, Specimens 10-3-
	1½
2.8-20	Transverse Reinforcement Unit Strains vs. Rotation, Specimens 10-3-
	1½
2.8-21	Transverse Reinforcement Unit Strains vs. Rotation, Specimens 10-3-3 185
2.8-22	Transverse Reinforcement Unit Strains vs. Rotation, Specimens 10-3-3 186
2.8-23	Transverse Reinforcement Unit Strains vs. Rotation, Specimens 10-3-
	21/4
2.8-24	Transverse Reinforcement Unit Strains vs. Rotation, Specimens 10-3-
	21/4
2.8-25	Transverse Reinforcement Unit Strains vs. Rotation, Specimens 20-3-
	1½
2.8-26	Transverse Reinforcement Unit Strains vs. Rotation, Specimens 20-3-
	1½
2.8-27	Transverse Reinforcement Unit Strains vs. Rotation, Specimens 20-3-3 191

Figure	Page
2.8-28	Transverse Reinforcement Unit Strains vs. Rotation, Specimens 20-3-3 192
2.8-29	Transverse Reinforcement Unit Strains vs. Rotation, Specimens 10-2-
	21/4
2.8-30	Transverse Reinforcement Unit Strains vs. Rotation, Specimens 10-2-
	21/4
2.8-31	Transverse Reinforcement Unit Strains vs. Rotation, Specimens 10-1-
	21/4
2.8-32	Transverse Reinforcement Unit Strains vs. Rotation, Specimens 10-1-
	21/4
2.9-1	Initial Unit Stress and Unit Strain Definition for Assumed Steel Unit
	Stress-Unit Strain Relationship
2.9-2	Estimated Compressive Force Acting on the Concrete, Specimens 10-2-
	3198
2.9-3	Estimated Compressive Force Acting on the Concrete, Specimens 10-3-
	1½198
2.9-4	Estimated Compressive Force Acting on the Concrete, Specimens 10-3-
	3199
2.9-5	Estimated Compressive Force Acting on the Concrete, Specimens 10-3-
	21/4
2.9-6	Estimated Compressive Force Acting on the Concrete, Specimens 20-3-
	1½200
2.9-7	Estimated Compressive Force Acting on the Concrete, Specimens 20-3-
	3200
2.9-8	Estimated Compressive Force Acting on the Concrete, Specimens 10-2-
	21/4
2.9-9	Estimated Compressive Force Acting on the Concrete, Specimens 10-1-
	21/4
2.10-1	Initial Responses of Specimens 10-2-3, 10-2-2 ¹ / ₄ and 10-1-2 ¹ / ₄
2.10-2	Initial Responses of Specimens 10-3-1½, 10-3-3 and 10-3-2 ¼

Figure	Page
2.10-3	Initial Responses of Specimens 20-3-3 and 20-3-1½
2.10.1-1	Effect of Hoop Spacing (10-2-21/4 North vs. 10-2-3 North)
2.10.1-2	Effect of Hoop Spacing (10-3-3 North vs. 10-3-2 ¹ / ₄ North)
2.10.2-1	Effect of Axial Load (10-3-3 North vs. 20-3-3 South)
2.10.2-2	Effect of Axial Load (10-3-11/2 South vs. 20-3-11/2 North)
2.10.3-1	Effect of Displacement History (10-3-21/4 North -no previous cycles-
	vs. 10-2-21/4 North -seven cycles at 2%- and 10-1-21/4 South -seven
	cycles at 1%-)
2.10.3-2	Effect of Displacement History (10-3-3 North vs. 10-2-3 North)
3.2-1	Angular Change Components
3.2-2	Displacement Components
3.2-3	Drift Ratio Calculated from Whittemore Readings, 10-2-3 North
3.2-4	Drift Ratio Calculated from Whittemore Readings,10-2-3 South
3.2-5	Drift Ratio Calculated from Whittemore Readings, 10-3-1½ North
3.2-6	Drift Ratio Calculated from Whittemore Readings, 10-3-11/2 South
3.2-7	Drift Ratio Calculated from Whittemore Readings, 10-3-3 North
3.2-8	Drift Ratio Calculated from Whittemore Readings, 10-3-3 South
3.2-9	Drift Ratio Calculated from Whittemore Readings, 10-3-21/4 North
3.2-10	Drift Ratio Calculated from Whittemore Readings, 10-3-21/4 South
3.2-11	Drift Ratio Calculated from Whittemore Readings, 20-3-11/2 North
3.2-12	Drift Ratio Calculated from Whittemore Readings, 20-3-11/2 South
3.2-13	Drift Ratio Calculated from Whittemore Readings, 20-3-3 North
3.2-14	Drift Ratio Calculated from Whittemore Readings, 20-3-3 South
3.2-15	Drift Ratio Calculated from Whittemore Readings, 10-2-21/4 North
3.2-16	Drift Ratio Calculated from Whittemore Readings, 10-2-21/4 South
3.2-17	Drift Ratio Calculated from Whittemore Readings, 10-1-21/4 North
3.2-18	Drift Ratio Calculated from Whittemore Readings, 10-1-21/4 South
3.2-19	Drift Ratio Components from Whittemore Readings, 10-2-3 North 217
3.2-20	Drift Ratio Components from Whittemore Readings, 10-2-3 South 217

Figure	Page
3.2-21	Drift Ratio Components from Whittemore Readings, 10-3-11/2 North 218
3.2-22	Drift Ratio Components from Whittemore Readings, 10-3-11/2 South 218
3.2-23	Drift Ratio Components from Whittemore Readings, 10-3-3 North 219
3.2-24	Drift Ratio Components from Whittemore Readings, 10-3-3 South 219
3.2-25	Drift Ratio Components from Whittemore Readings, 10-3-21/4 North 220
3.2-26	Drift Ratio Components from Whittemore Readings, 10-3-21/4 South 220
3.2-27	Drift Ratio Components from Whittemore Readings, 20-3-11/2 North 221
3.2-28	Drift Ratio Components from Whittemore Readings, 20-3-11/2 South 221
3.2-29	Drift Ratio Components from Whittemore Readings, 20-3-3 North 222
3.2-30	Drift Ratio Components from Whittemore Readings, 20-3-3 South 222
3.2-31	Drift Ratio Components from Whittemore Readings, 10-2-21/4 North 223
3.2-32	Drift Ratio Components from Whittemore Readings, 10-2-21/4 South 223
3.2-33	Drift Ratio Components from Whittemore Readings, 10-1-21/4 North 224
3.2-34	Drift Ratio Components from Whittemore Readings, 10-1-21/4 South 224
3.3-1	Shear Distortion ν , 10-2-3 North
3.3-2	Shear Distortion <i>v</i> , 10-2-3 South
3.3-3	Rotation θ , 10-2-3 North. 226
3.3-4	Rotation θ , 10-2-3 South. 226
3.3-5	Shear Distortion ν , 10-3-1½ North
3.3-6	Shear Distortion ν , 10-3-1½ South
3.3-7	Rotation θ , 10-3-1½ North. 228
3.3-8	Rotation θ , 10-3-1½ South. 228
3.3-9	Shear Distortion ν , 10-3-3 North
3.3-10	Shear Distortion ν , 10-3-3 South
3.3-11	Rotation θ , 10-3-3 North. 230
3.3-12	Rotation θ , 10-3-3 South. 230
3.3-13	Shear Distortion <i>v</i> , 10-3-2 ¹ / ₄ North
3.3-14	Shear Distortion <i>v</i> , 10-3-2 ¹ / ₄ South

Figure	Page
3.3-15	Rotation θ , 10-3-2 ¹ / ₄ North. 232
3.3-16	Rotation θ , 10-3-2½ South. 232
3.3-17	Shear Distortion <i>v</i> , 20-3-1½ North
3.3-18	Shear Distortion ν , 20-3-1½ South
3.3-19	Rotation θ , 20-3-1½ North. 234
3.3-20	Rotation θ , 20-3-1½ South. 234
3.3-21	Shear Distortion ν , 20-3-3 North
3.3-22	Shear Distortion <i>v</i> , 20-3-3 South
3.3-23	Rotation θ , 20-3-3 North
3.3-24	Rotation θ , 20-3-3 South
3.3-25	Shear Distortion <i>v</i> , 10-2-2 ¹ / ₄ North
3.3-26	Shear Distortion ν , 10-2-2½ South
3.3-27	Rotation θ , 10-2-2½ North
3.3-28	Rotation θ , 10-2-2½ South
3.3-29	Shear Distortion <i>v</i> , 10-1-2 ¹ / ₄ North
3.3-30	Shear Distortion ν , 10-1-2½ South
3.3-31	Rotation θ , 10-1-2½ North
3.3-32	Rotation θ , 10-1-2½ South
3.3-33	Concrete Core Expansion and Shear Distortion
3.4-1	Calculated Moment-Curvature Relationships
3.4-2	Idealized Steel Unit Strain - Unit Stress Relationship Used for
	Calculation of Average Bond Stresses and Moment-Curvature
	Relationships. 243
3.4-3	Idealized Concrete Unit Strain - Unit Stress Relationship Used for
	Calculation of Moment-Curvature Relationships
3.4-4	Assumed distribution of Unit Strains and Unit Stresses in Bars
	Embedded in the Center Stub. 245
3.4-5	Average Bond Stresses

Figure		Page
3.4-6	Drift Ratio Related to Shear vs. Drift Ratio Related to Bending and Slip.	246
3.4-7	Measured vs. Calculated Drift Ratio.	247
3.4-8	Measured vs. Calculated Drift Ratio.	247
3.4-9	Measured vs. Calculated Drift Ratio.	248
4.2-1	Typical Transverse Deformation History	249
4.2-2	Idealized Transverse Deformation vs. Drift Ratio Relationship	250
4.4-1	Model B Geometry.	251
4.4-2	Model B Geometry: Close-up.	252
4.4-3	Model B Geometry: Deformation Components.	253
4.4-4	Measured and Calculated Values of Strain in Longitudinal Bars	254
4.4-5	Measured and Calculated Values of Strain in Longitudinal Bars	254
4.4-6	Measured Values of Strain in Longitudinal Bars.	255
4.4-7	Measured Values of Strain in Longitudinal Bars.	255
4.4-8	Calculated Values of Strain in Longitudinal Bars (10in. from base)	256
4.4-9	Measured and Calculated Strains in Longitudinal Bars (10in. from	
	base).	256
4.5-1	Measured vs. Calculated Number of Cycles, Model A	257
4.5-2	Measured vs. Calculated Number of Cycles, Model B.	257
4.6-1	Maximum Drift Ratio vs. Parameter k_1 .	258
4.6-2	Idealized Displacement Schedule Used to Project Data from This	
	Investigation	258
4.6-3	Maximum Drift Ratio vs. Parameter k_1 , Comparison of Data Obtained	
	in Previous Experiments with Projections from Observations Made in	
	This Study.	259
4.7-1	Force-Displacement Relationship Adopted for Reference SDOF	
	System.	260
4.7-2	EW Ground Acceleration, El Centro Record Scaled to 0.4g Peak	
	Ground Acceleration, Imperial Valley, 1940 Earthquake	261

Figure		Page
4.7-3	Estimated Maximum Inter-Story Drift Ratio for an Idealized 10-Story	
	RC Frame Building, El Centro, Imperial Valley, 1940 Earthquake, EW	
	Component Scaled to 0.4g.	262
4.7-4	Estimated Maximum Inter-Story Drift Ratio for an Idealized 20-Story	
	RC Frame Building, El Centro, Imperial Valley, 1940 Earthquake, EW	
	Component Scaled to 0.4g.	263
4.7-5	Estimated Maximum Inter-Story Drift Ratio for an Idealized 30-Story	
	RC Frame Building, El Centro, Imperial Valley, 1940 Earthquake, EW	
	Component Scaled to 0.4g.	264
4.7-6	EW Ground Acceleration, Secretaría de Transporte Record Scaled to	
	0.4g Peak Ground Acceleration, Mexico City, Mexico, 1985	
	Earthquake	265
4.7-7	Estimated Maximum Inter-Story Drift Ratio for an Idealized 10-Story	
	RC Frame Building, Secretaría de Transporte, Mexico City, Mexico,	
	1985 Earthquake, EW Component Scaled to 0.4g.	266
4.7-8	Estimated Maximum Inter-Story Drift Ratio for an Idealized 20-Story	
	RC Frame Building, Secretaría de Transporte, Mexico City, Mexico,	
	1985 Earthquake, EW Component Scaled to 0.4g.	267
4.7-9	Estimated Maximum Inter-Story Drift Ratio for an Idealized 30-Story	
	RC Frame Building, Secretaría de Comunicaciones y Transporte,	
	Mexico City, Mexico, 1985 Earthquake, EW Component Scaled to	
	0.4g	268
4.7-10	Nine-Story Building Model with a "Soft-Story", Moehle, 1980	269
4.7-11	First-Story Drift-Ratio Response, Nine-Story Building Model with a	
	"Soft-Story" Subjected to Base Accelerations Modeled After the N-S	
	Component of the El Centro 1940 Record Scaled to 0.4g Peak Ground	
	Acceleration, Moehle, 1980.	270
Appendix Figure		
A.2.1-1	Compressive Strength, Concrete Batch 1	285

Appendix	Figure Page	Э
A.2.1-2	Compressive Strength, Concrete Batch 2	
A.2.1-3	Compressive Strength, Concrete Batch 3	,
A.2.1-4	Initial Stress-Strain Curves for Concrete Cylinders, Specimens 10-2-3 286	,
A.2.1-5	Initial Stress-Strain Curves for Concrete Cylinders, Specimens 10-3-	
	1½	,
A.2.1-6	Initial Stress-Strain Curves for Concrete Cylinders, Specimens 10-3-3 287	,
A.2.1-7	Initial Stress-Strain Curves for Concrete Cylinders, Specimens 10-3-	
	21/4	,
A.2.1-8	Initial Stress-Strain Curves for Concrete Cylinders, Specimens 20-3-	
	1½	;
A.2.1-9	Initial Stress-Strain Curves for Concrete Cylinders, Assembly 20-3-3 289)
A.2.1-10	Initial Stress-Strain Curves for Concrete Cylinders, Assembly 10-2-	
	21/4)
A.2.1-11	Initial Stress-Strain Curves for Concrete Cylinders, Assembly 10-1-	
	21/4)
A.2.1-12	Concrete Modulus of Elasticity vs. Compressive Strength)
A.2.1-13	Concrete Tensile vs. Compressive Strength	
A.2.1-14	Effect of Grinding Longitudinal Deformations	
A.2.1-15	Partial Stress-Strain Curves for ¼-in Diameter Bars	•
A.2.1-16	Partial Stress-Strain Curves for ¾-in Diameter Bars. 292	,
A.3.1-1	Test Assembly: Nominal Dimensions (in Inches) and Reinforcement	
	Details	i
A.3.2-1	Support for Bronze Bushings to be Cast in the Concrete	•
A.3.2-2	Confinement Reinforcement in Support Region. 294	
A.3.3-1	Reinforcement Cage Placed in Steel Form Before Casting	
A.3.3-2	Molds Prepared for Casting	
A.3.3-3	Steel Form Prepared for Casting. 296	
A.3.3-4	Placing of Concrete in Form. 296	;
A.3.3-5	Vibration of Concrete	,

Appendix Figure		Page
A.3.3-6	Leveling of Concrete.	297
A.3.3-7	Curing.	298
A.4.1-1	Loading Frame.	299
A.4.1-2	Loading Frame.	299
A.4.1-3	PVC Pipes Sealed and Ready for Concrete Casting.	300
A.4.1-4	Post-Tensioning of Center Stub.	300
A.4.1-5	End Support.	301
A.4.1-6	Lateral Bracing.	302
A.4.1-7	Rollers on Lateral Braces.	302
A.4.1-8	External Post-Tensioning System.	303
A.4.1-9	Rams Applying Axial Load	303
A.4.1-10	Load Cells Used to Control Axial Load.	304
A.4.1-11	End Swivel.	304
A.4.2-1	Location of Deflection Measurements (Dimensions in Inches)	305
A.4.2-2	Calculation of Center Stub Rotation (a) and Drift Ratio Definition	306
A.4.2-3	Instrumented 1/4-in Hoop.	307
A.4.2-4	Strain Gages Location.	307
A.4.2-5	Mesh of Whittemore Reference Points (Dimensions in Inches)	308
A.4.3-1	EA-06-125HN-120 Electrical Strain Gage.	308
A.4.3-2	Strain Gages Prepared for Concrete Casting	309
A.4.3-3	Whittemore Gage.	309

ABSTRACT

Pujol, Santiago Ph.D., Purdue University, August 2002. Drift Capacity of Reinforced Concrete Columns Subjected to Displacement Reversals. Major Professors: Julio A. Ramirez and Mete A. Sozen.

In previous tests of columns under displacement reversals in the inelastic range of response, different arbitrary displacement histories have been used. Comparisons of drift-capacity data from columns tested under different displacement histories can only be made if displacement-history effects are ignored. Possibly because of this reason, currently available methods for column drift capacity ignore displacement-history effects. To investigate whether drift capacity is a function of displacement history, sixteen cantilever columns were tested under various displacement patterns. The test results indicate that column drift capacity is sensitive to displacement history. For columns cycled beyond yield, drift capacity decreases as a function of the amplitude and number of cycles the column has experienced. Based on measurements of average unit strains in the transverse reinforcement, a model is proposed for estimating the drift capacity for a given column under any symmetric displacement pattern.

1 INTRODUCTION

1.1 Background

The essential requirement for a reinforced concrete column of a structure to resist strong ground motion is that it retains a substantial portion of its strength as it experiences displacement reversals in the nonlinear range of response. This study addresses the problem of estimating column deformation capacity considering possible displacement-history effects.

1.2 Previous Investigations

There is abundant information on the behavior of reinforced concrete columns under displacement reversals (Taylor et al., 1993 and 1997; Eberhard, 2000). Several studies have been focused on the possible effects of displacement history. Blume et al. (1961) recognized that for elements of reinforced concrete buildings "only a few yield excursions are expected to occur in one earthquake even of long duration." For this reason, and referring to results of tests of beams subjected to one inelastic displacement reversal, it was suggested that the effect of displacement reversals on the drift capacity of a reinforced concrete member can be generally ignored in design of buildings for earthquakes. But in the 1970s, experimental results (Wight and Sozen, 1973) indicated that repeated displacement reversals may cause a severe reduction in column stiffness. Many studies that followed led to similar results, but just a few of these studies addressed the problem of possible displacement-history effects. Murakami and Imai (1986) tested four similar columns under constant axial load and different displacement histories and observed a more rapid reduction in column stiffness for displacement histories with larger numbers of cycles per displacement increment. In these columns, the maximum nominal unit shear stress (ratio of shear force to the product of cross-sectional width times

effective depth) was of the order of $3\sqrt{f_c'}$, where f_c' is the compressive strength of the concrete and all unit stresses are expressed in psi. The failure process of these columns was dominated by buckling of the longitudinal reinforcement under compression. Iwasaki et al. (1987) tested 7 reinforced concrete members with varying aspect ratios under displacement histories with 3 to 10 cycles per displacement increment. The columns with higher maximum nominal unit shear stresses (of the order of $4\sqrt{f_c'}$) showed a more rapid decrease in stiffness and increase in transverse reinforcement unit strains for larger number of cycles per displacement increment. Park (1989) recommended a procedure for testing reinforced concrete columns under displacement reversals to assess drift capacity based on results from analytical studies (Mahin and Bertero, 1981) on the response of nonlinear SDOF systems to strong ground motion. Park proposed that the drift capacity, Δ_{max} , of a column tested under any given symmetric displacement schedule be determined by the expression

$$\Delta_{max} = \frac{1}{4} \int_{i=1}^{n} \Delta_i$$
 (1.2-1)

where

 Δ_i : maximum drift for displacement cycle i,

n number of cycles applied prior to a decrease in strength of more than20%.

El-Bahy et al. (1999) tested relatively slender columns (ratio of shear span to diameter of 4.5) with circular cross-sections under displacement cycles of constant amplitude. The failure modes observed were dominated by buckling and fracture of longitudinal reinforcement. The total number of cycles of constant amplitude that a column could sustain before failure was observed to decrease with increasing cycle amplitude. Ingham et al. (2001) tested beams under low maximum nominal unit shear stresses (less than $2\sqrt{f_c'}$) and different displacement schedules and observed the maximum drift reached before strength decay to decrease with increasing number of cycles per displacement increment.

Possibly because of the scarcity of relevant data, current analytical models for the drift capacity of reinforced concrete columns whose responses may be expected to be dominated by shear effects (Aoyama, 1993; Moehle et al. 2000, Priestley et al. 1994; FEMA 273, 1997; Aschheim, 2000) ignore possible displacement-history effects.

1.3 Objective and Scope

The objective of the study described in this report is to determine whether the displacement history has an effect on the drift capacity of a reinforced concrete column under displacement reversals in the inelastic range of response. Columns susceptible to shear or bond failures before reaching the full flexural capacity are not considered. Special attention is given to columns under relatively high nominal shear stresses (large enough to cause inclined cracking before yielding of the longitudinal reinforcement). This study and its results are limited to the following cases:

- 1) Drift cycles occur primarily in the plane defined by one of the principal axes of the cross section.
- 2) The drift capacity is not less than the drift at yield.
- 3) The maximum shear exceeds the shear at inclined cracking.
- 4) The "static" shear capacity is not less than the shear at yield.
- 5) The column core is effectively confined by transverse reinforcement.
- 6) Longitudinal reinforcement is restrained against buckling by transverse reinforcement.

The variables considered are:

Maximum nominal unit shear stress $V/(b d \sqrt{f'_c})$: 6 to 8 (unit stresses in psi)

Maximum core unit shear stress, $V/(A_c\sqrt{f_c'})$: 10 to 13 (unit stresses in psi)

Axial load (kept constant in each test), P: 0.08 to 0.21 $f'_c A_g$ (30-60 kips)

Transverse reinforcement ratio, $A_W/(bs)$: 0.6% to 1.1%

Nominal unit transverse stress, $A_w f_{yw} / (b_c s)$: 500 to 1000 psi

Maximum drift ratio – ratio of displacement to shear span–, γ_{max} : 3%-4%

The constants are as follows:

Concrete compressive strength, f_c : 4.1 to 5.2 ksi

Longitudinal reinforcement unit yield stress, f_y : 65.7 ksi

Longitudinal reinforcement ratio, ρ : 2.4%

Ratio of shear span a, to effective depth d: 2.7

Ratio of gross cross-sectional area A_g , to core area A_c : 2.0

where

V : maximum shear force,b : cross-sectional width.

d : effective depth,

 A_{w} : total cross-sectional area in a layer of transverse reinforcement,

 f_{vw} : transverse reinforcement unit yield stress,

 b_c : concrete core cross-sectional width (measured center-to-center of

exterior transverse reinforcement),

 A_c : concrete core cross-sectional area (measured center-to-center of

exterior transverse reinforcement),

s : hoop spacing.

1.4 Preliminary Criterion for Classification of Available Data

At the beginning of the investigation that includes this study, available data from different investigations were classified using the criterion that is described next (Pujol et al., 2000). In the formulation developed, the failure criterion proposed by Coulomb (1773) for materials under shear (τ) and unit normal stresses (σ) acting in one plane is used to estimate the strength of the concrete in the core of a column under displacement reversals. The average state of stresses in the column core is represented using a Mohr circle for average unit stresses (Figure 1.4-1). The average unit axial stress is taken as:

$$\sigma_a = \frac{P + \frac{1}{2}A_s f_y}{h_c \cdot b_c} \tag{1.4-1}$$

Average unit transverse stresses are computed based on the properties of the transverse reinforcement:

$$\sigma_t = \frac{A_w f_{yw}}{s \cdot b_c} \tag{1.4-2}$$

Unit shear stresses are computed as:

$$\tau = \frac{V}{h_C \cdot b_C} \tag{1.4-3}$$

where

P : axial load,

 A_s : total cross-sectional area of longitudinal reinforcement,

 f_{V} : longitudinal reinforcement unit yield stress,

 h_c : concrete core depth (measured center-to-center of the transverse

reinforcement),

 b_c : concrete core width (measured center-to-center of the transverse

reinforcement),

V : maximum shear force,

s : hoop spacing,

 A_w : transverse reinforcement total cross-sectional area,

 f_{vw} : transverse reinforcement unit yield stress.

Failure is assumed to occur when the Mohr circle for average unit stresses intersects the line described by the expression:

$$\tau = k_1 \cdot f_c' + k_2 \cdot \sigma \tag{1.4-4}$$

where f'_c is the compressive strength of the concrete.

The initial values of coefficients k_1 and k_2 are defined, based on the work by Richart (1929), as $k_1 = 1/4$ and $k_2 = 3/4$. It is assumed that the strength of the concrete in the core of the column decreases with increasing number of displacement cycles of large amplitude and that this reduction in strength can be modeled by reducing coefficient k_1 .

Because of the lack of relevant information, the assumed reduction in k_1 was calibrated ignoring possible displacement-history effects. The reduction in k_1 was calibrated with respect to drift ratio capacity (the maximum drift ratio –ratio of displacement to shear span– reached before a reduction in strength exceeding 20%) and the ratio of shear span to effective depth (λ). Data reported by Ohue et al. (1985), Ono et al. (1989), Saatcioglu and Ozcebe (1989), Sakai et al. (1990), Wight (1973), and Xiao and Martirossyan (1998) were organized as shown in Figure 1.4-2 to allow selection of the rate at which k_1 is assumed to decrease with increasing maximum displacement:

$$k_1 = \frac{1}{7} \left(1 - \frac{100}{3} \frac{\gamma_{max}}{\lambda} \right) \ge 0$$
 (1.4-5)

Table 1.4-1 and Figures 1.4-3 to 1.4-5 show relevant properties of the specimens considered. The ranges of the data in Figure 1.4-2 are:

Concrete compressive strength, f'_c : 3,700 to 14,000 psi

Longitudinal reinforcement unit yield stress, f_v : 49,000 to 74,000 psi

Longitudinal reinforcement ratio, ρ : 2% to 3.6%

Nominal core unit shear stress, $V/(A_c\sqrt{f_c'})$: 6 to 13 (unit stresses in psi)

Axial load, P: 0.07 to 0.35 $f'_c A_g$.

Nominal unit transverse stress, $A_w f_{yw} / (b_c s)$: 240 to 1,400 psi

Ratio of shear span a, to effective depth d: 1.9 to 3.5

Ratio of gross cross-sectional area A_g , to core area A_c : 1.3 to 2.0

Maximum drift ratio, $\gamma_{max} = \Delta_{max} / a$: 1 to 9%

where

V : maximum shear force,

 A_w : total cross-sectional area in a layer of transverse reinforcement,

 f_{VW} : transverse reinforcement unit yield stress,

 b_c : width of the concrete core measured center-to-center of exterior

transverse reinforcement,

 A_c : cross-sectional area of the concrete core measured center-to-center of exterior transverse reinforcement,

s : hoop spacing.

 Δ_{max} : maximum drift reached before a reduction in strength exceeding 20%.

Failure, i.e., intersection between the reduced strength line and the Mohr circle for average unit stresses, requires:

$$\frac{\sigma_t}{\sigma_a} = \frac{3}{8}\alpha + 1 - \frac{5}{8}\sqrt{\alpha^2 - \beta^2}$$
 (1.4-6)

where
$$\alpha = 4 \frac{k_1 \cdot f'_c}{\sigma_a} + 3$$
 and $\beta = 4 \frac{\tau}{\sigma_a}$.

 σ_a : average unit axial stress,

 σ_t : average unit transverse stress,

 τ : average unit shear stress,

 k_1 : parameter that represents the strength of the concrete in the column core. It is defined in Figure 1.4-1. Coefficient k_1 is assumed to decrease with displacements reversals as indicated by Equation 1.4-5.

 f'_c : concrete compressive strength.

These expressions can be used either to determine the amount of transverse reinforcement required for columns to resist cycles of displacement of known amplitude or to evaluate the deformation capacity of existing columns.

The experiments carried out as part of this investigation were designed to test the hypothesis, implicit in this and other available analytical models (Aoyama, 1993; Moehle et al. 2000, Priestley et al. 1994; FEMA 273, 1997; Aschheim, 1997), that column drift capacity is independent of displacement history.

2 EXPERIMENTS

2.1 Introduction

The experimental program included a total of eight test assemblies. An assembly consisted of two test specimens joined by a center stub. Each specimen was intended to represent a cantilever column under axial load and a point transverse load applied at its end. The center stub was intended to act as the base of the cantilevers (Figure 2.1-1).

The cross section of the specimens was 6-in. wide and 12-in. deep and the shear span (a; distance from the support point to the nearest face of the center stub) was 27 in. The effective depth (d) was 10 in., for a shear span to effective depth ratio (a/d) of 2.7. The longitudinal reinforcement consisted of four continuous $\frac{3}{4}$ -in. diameter bars with an average unit yield stress of 65.7 ksi. Transverse reinforcement outside the center stub consisted of hoops made from plain $\frac{1}{4}$ -in diameter bars with an average unit yield stress of 59.6 ksi. Average concrete strength ranged from 4100 to 5200 psi. Details about the dimensions of the specimens and the properties of the materials used are given in the Appendix.

The variables controlled in the experiments were the spacing of the hoops outside the center stub, the axial load, and the displacement history. The spacing of the hoops outside the joint was either 1½, 2¼ or 3 inches. The axial load was either 30 or 60 kips. The complete experimental program, including the displacement history for each test assembly described in terms of maximum drift ratio, is presented in Table 2.1-1. Relative rotation, or drift ratio, is defined in Figure A.4.2-2. The rotation of only one of the two specimens per test assembly could be controlled. As the tests progressed, damage, stiffness reduction, and rotation concentrated in one of the two cantilevers per test assembly. The displacement at mid-span was controlled so that the larger of the two specimen rotations did not exceed the target maximum drift ratio. Relative-rotation

targets were 1, 2, 3, and 4%. All tests were carried out until a reduction in lateral stiffness of 50 % or more was observed.

All assemblies are designated using three numerals. The first numeral indicates the level of axial load as a percentage of the product $f'_c \cdot A_g$ (where f'_c is the compressive strength of the concrete and A_g is the gross cross-sectional area). The second numeral indicates the maximum drift ratio to be reached during the initial displacement cycles. The last numeral is the hoop spacing in inches.

As described in the Appendix, the measurements taken during the tests included:

- transverse and axial load,
- deflections,
- rotations,
- unit strains in the transverse and longitudinal reinforcement,
- deformations of the concrete surface,
- and crack widths.

Electronic Whittemore gages were used to measure the changes in distance between steel discs epoxy-glued to the concrete surface on the west side of each test assembly. The measurements made and the array of reference points are shown in Figure A.4.2-5. Reference to these measurements will be made using the labels shown in Figure 2.1-2.

Additional information on the experimental program is given in the Appendix.

2.2 Observed Shear-Drift Ratio Response

Figures 2.2-1 to 2.2-16 show the shear-drift ratio curves recorded. Drift ratio is defined in Figure A.4.2-2. Positive loads and rotations correspond to downward deflections (see the Appendix for a description of the loading frame).

All specimens developed inclined cracks before yielding of the longitudinal reinforcement. All specimens reached their full flexural capacity and inelastic deformations.

2.2.1 First Displacement Cycle

The behavior of all specimens during the first displacement cycle was similar. Under positive loads, cracks perpendicular to the column axis were first observed at a shear force of about 5.5 to 6.5 kips for the specimens with a 30-kip axial load. For the specimens under a 60-kip axial load, first cracking was observed at approximately 10.5 kips. Flexural cracks started to deviate from the vertical at shear forces of about 20 to 22 kips for specimens with a 30-kip axial load. Flexural cracks started to deviate from the vertical at 27 kips for specimens 20-3-1½ and at 30 kips for specimens 20-3-3. Yielding was reached consistently at a drift ratio of approximately 1% (see Figures 2.2-1 to 2.2-16). At that point, light spalling of the concrete under compression was already visible (Figure 2.2.1-1). Specimens with a higher axial load showed concrete spalling over a larger area (Figure 2.2.1-2).

Under negative (upward) loads, small inclined cracks formed in between cracks from the previous half displacement cycle in specimens 10-3-1½, 10-3-3, 10-3-2¼ and 10-2-2¼ at shear forces ranging from 5 to 6.5 kips. In the other specimens under a 30-kip axial load, flexure-shear cracks started to develop at shear forces ranging from 9 to 10 kips. Specimens 20-3-3 developed small inclined cracks between existing cracks at a shear force of 10 kip. Flexure cracks were observed to deviate from the vertical at 13 kips for specimens 20-3-1½. Spalling of the concrete shell was typically less pronounced at the bottom than at the top of the specimens (Figure 2.2.1-3) during the first displacement cycle.

Figures 2.2.1-4 to 2.2.1-11 show the cracking pattern observed at different stages during the first cycle for all the specimens. Black lines drawn on the concrete surface show the location of cracks. Hatched areas indicate bulges on the concrete surface.

2.2.2 Subsequent Cycles

Table 2.2.2-1 presents numbers of figures showing the state of the specimens at different test stages. Again, black lines drawn on the concrete surface show the location of cracks and bulges are hatched. For all specimens, additional cycles at drift ratios exceeding 1% caused widening of inclined cracks and, consequently, a permanent

increase in the depth of the cross-sections near the column base. Progressive damage of the concrete shell and core was also observed. The larger the maximum drift ratio, the faster was the disintegration and expansion of the concrete. Stiffness decrease and damage accelerated during the last loading cycles.

During the second half of cycle eight for Specimens 20-3-1½, a power failure caused loss of hydraulic pressure in the MTS system. Lateral load dropped to zero when the specimens were at a drift ratio of approximately –3% (Figures 2.2-9 and 2.2-10). Data were not lost. During the second half of cycle 17, buckling of the top longitudinal bars at the north joint face, (Figure 2.2.2-14) caused a sudden reduction in the lateral stiffness of the north specimen. By that time, spalling of concrete had penetrated far into the center joint (Figure 2.2.2-15). Because the No. 2 hoops near the face of the joint may have already been yielding (Figures 2.7-17 and 2.7-19), and because the No.3 hoops in the joint did not support the longitudinal bars effectively, once the concrete shell was lost nothing could restrain the longitudinal reinforcement against buckling at the face of the joint. Because this mode of failure is not representative of the problem under study, the results for Specimens 20-3-1½ are not included in following discussions about stiffness reduction with number of cycles.

2.3 Failure

Figures 2.3-1 to 2.3-7 show details of specimens after failure. Failure was characterized by expansion and disintegration of the concrete within a distance of 10 in. from the column base.

After completion of the tests, the axial load was increased to 80 kips for all the test assemblies. To avoid increasing second-order moments, the MTS actuator was used to keep the final permanent lateral deflection constant as the axial load was increased. All the specimens were able to sustain the 80-kip axial load applied. Following this additional test, loose concrete was removed to determine the extent of the damage in each specimen. Figures 2.3-8 to 2.3-19 show specimens after removal of the loose concrete. Observe that, after failure, all the concrete within the "plastic hinge" had been reduced to a collection of broken fragments. This collection of fragments was able to carry some

axial and transverse load because of the friction between fragments and the confinement still provided by the reinforcing cage despite the fact it had expanded.

2.4 Stiffness vs. Number of Cycles

Stiffness is defined here as the slope of the line joining the peaks of the shear-drift ratio curve for a given cycle. The peaks of a displacement cycle are defined as the two points most distant to the origin on a shear force (V) versus drift ratio (γ) plot. Distance to the origin (d_0) is defined as:

$$d_o = \sqrt{V^2 + (1000 \cdot \gamma)^2} \tag{2.4-1}$$

Figures 2.4-1 to 2.4-8 show the stiffness vs. number of cycles response for specimens where damage concentrated and for cycles at the maximum target drift ratio. The variation of stiffness with number of cycles shown for specimen 20-3-1½ North is limited to cycles applied before buckling of the longitudinal reinforcement at the joint face.

In Figures 2.4-1 to 2.4-8, lower target drift ratios are associated with higher values of initial stiffness because, after yielding, the lateral load applied to the system remains practically constant for increasing values of maximum drift.

For cycles of displacement in the inelastic range, the response of the specimens was never stable. Stiffness decay with increasing number of cycles was always present for cycles at drift ratios larger than 1%. The rate at which stiffness decreases increases with increasing number of displacement cycles. The final rate of stiffness decrease is a function of the level of axial load. The higher axial load caused more abrupt stiffness loss during the final displacement cycles.

Specimens with a hoop spacing of 3 in. and a 30-kip axial load (10-2-3 and 10-3-3) showed a rapid decrease in stiffness with cycles at a drift ratio of 3%. On the other hand, specimens with a hoop spacing of 1½ in. (10-3-1½) showed a very stable behavior for a large number of cycles at a drift ratio of 4%. Specimens with a 2¼ in. hoop spacing failed also in a very gradual manner but at a maximum drift ratio of 3%.

Similar specimens tested under different displacement schedules showed differences in behavior. Specific comparisons are discussed in Section 2.10.

Because of the gradual nature of the failure process, a criterion had to be adopted to classify the response of a specimen during a given cycle. In Figures 2.4-1 to 2.4-8, a horizontal line has been drawn at 80% of the initial stiffness value. The numbers of the cycles at the intersection of this line and the curve relating stiffness to number of cycles are tabulated in Table 2.4-1. In this study, the boundary, in terms of number of cycles, between adequate and inadequate response is defined by the number of cycles at which this intersection occurred.

2.5 Transverse Deformations

The relative movement between reference points at three different cross-sections was measured using Whittemore gages (described in the Appendix). The cross-sections were numbered sequentially from the base to the end of the specimens (Figure 2.1-2). Section 1 is at four inches from the base. Sections 2 and 3 are at 8 and 16 in. from the base, respectively. At sections 1 and 2, the total change in the distance between the outmost points was obtained as the sum of two measurements made with a 4-in. gage. At section 3, an 8-in. gage was used. To check the consistency of these measurements, a redundant measurement was made at section 2 with the 8-in gage. This measurement was compared with the sum of the two measurements made with the 4-in. gage. Figures 2.5-1 to 2.5-16 show the sectional depth change at cycle peaks measured at sections 1-3 for all the specimens tested. Extensions are plotted as positive values. Observe that the two measurements made at section 2 matched in all the tests.

In general, the largest transverse deformations were measured at section 1. For all specimens, transverse deformations increased at an increasing rate with additional cycles. This rate was a function of: 1) the amount of transverse reinforcement, 2) the axial load and 3) the displacement history. The larger the displacement amplitude, the larger was the increase in transverse deformations.

The vertical solid line in Figures 2.5-1 to 2.5-16 refers to the cycle at which a drop in stiffness of 20% or more was first measured. Observe that a stiffness loss of

more than 20% was consistently measured only after transverse deformations larger than 0.25 in (3% average unit strain) had taken place. This is better illustrated in Figure 2.5-17. In this figure, the horizontal axis represents the cycle at which a transverse deformation of 0.25 in. or more was first measured (Table 2.4-1). The vertical axis represents the cycle when a drop in stiffness of 20% or more was first measured. From the trend observed, it can be concluded that excessive stiffness loss was caused by displacement reversals only after transverse deformations exceeded 0.25 in. (3% average unit strain). This observation ties the overall response of a specimen under any given loading pattern to a single simple variable that can be measured easily.

Figures 2.5-18 to 2.5-25 show comparisons of transverse deformations and maximum width of inclined cracks (measured with a crack comparator). These two variables are not directly comparable because several cracks may have crossed a given cross-section and because the measurements were made in different directions. Crack widths were measured in the direction perpendicular to each crack at its widest point while transverse deformations were measured along sections perpendicular to the column axis. Recognizing these differences in direction, a general conclusion can still be made. During the initial cycles, opening of cracks is due mainly to extension of fibers parallel to the column axis. During subsequent cycles, crack widths include a component of increasing magnitude related to extension of fibers perpendicular to the column axis.

2.6 Longitudinal Reinforcement Unit Strains

Figures 2.6-1 to 2.6-16 show the unit strain values measured on the longitudinal reinforcement at the locations instrumented in all the specimens tested. Tensile strains are plotted as positive values. Except for specimens with the higher axial load, the strains measured at the joint face were tensile for displacement cycles following the first cycle. This may imply that the concrete core expanded as it fractured and particles rearranged or that the cracks at the joint face never closed completely and the steel carried all compressive forces. Progressive crushing of the concrete at the joint face observed during the tests supports the first hypothesis and refutes the second. A study of the average internal forces in the plastic hinge region is presented in Section 2.9.

The strain gages at the joint face also showed a systematic reduction in the maximum unit strain reached during excursions of displacement causing tension in the corresponding reinforcement, indicating that displacement reversals caused a reduction in the magnitude of the curvature at this section. Because the amplitude of the cycles applied was kept constant, this implies that the relative magnitude of flexural deformations decreased while the relative magnitude of other deformation components increased. A study of the magnitude and the history of deformation components is presented in Chapter 3.

2.7 Hoop Unit Strains

Figures 2.7-1 to 2.7-32 show the unit strain values measured on the instrumented hoops. Tensile strains are plotted as positive values. As opposed to the measurements of transverse deformation obtained with the Whittemore gages, not all the measurements from electrical strain gages show continuous accumulation of unit strains for cycles at drift ratios exceeding 1%. Because the steel used to fabricate the hoops has a well-defined yield plateau, it can be inferred that hoop unit strains concentrated where the hoops intersected the inclined cracks. But accumulation of hoop strains with displacement reversals did happen in some locations in all the specimens. Consistently, this "ratcheting" was always observed during the final loading cycles. The start of the ratcheting process did not coincide with the point at which the measured unit strain reached the unit yield strain. Strain gages placed on the horizontal legs of the second hoop from the joint showed ratcheting too, indicating that the change in the volume of the concrete core caused by the load reversals was three-dimensional.

2.8 Rotation

In each specimen, Whittemore reference points were arranged in three 8x8-in. squares (Figure A.4.2-5). One of these squares was located within the center stub, its outermost side coinciding with the face of the joint. Adjacent squares shared one vertical gage line. The squares were numbered from the center stub out and they will be referred to as "gage locations." Within each gage location, rotation was calculated as the ratio of

the difference between the two horizontal measurements to the nominal height of the square (8 in.). The total rotation at the section defined by one of the vertical sides of a square was calculated as the sum of the rotations in the gage locations in between that section and the center of the test assembly. The total rotation at 8-in. from the joint face was calculated as the sum of the rotations in gage locations 1 and 2. Figures 2.8-1 to 2.8-16 show rotation plotted against applied drift ratio. Rotations are plotted as positive values when corresponding to extension at the bottom and compression at the top of the specimen. For a given cycle, the relationship between drift and rotation at 8 in. from the column base appears to be linear. Not enough data were recorded to make definite observations on the change of the nature of this relationship with increasing number of cycles. Whittemore data were recorded until the loss of reference points caused by disintegration of the concrete or until the deformations exceeded the range of the instruments. Generally, the points affected first by crushing of the concrete were those located at the face of the joint.

Figures 2.8-17 to 2.8-32 show selected strain gage measurements plotted versus rotation at 8 in. from the base. Because the relationship between rotation and drift ratio was linear for the measurements made, these plots reveal no additional trends.

2.9 Internal Forces

Except for specimens with the higher axial load, the strains measured with electrical strain gages cemented to the longitudinal bars at the joint face were tensile for displacement cycles following the first cycle. Permanent tensile deformations in the longitudinal bars would occur if the concrete core expands as it fractures and particles rearrange or if the cracks at the joint face never close completely and the steel carries all compressive forces. Forces in the steel were estimated using average strains calculated by dividing the top and bottom horizontal Whittemore measurements at location 2 by the nominal gage length (8 in.). Because each steel layer was subjected to alternating tensile and compressive forces, a hysteretic model for the relationship between unit strains and unit stresses had to be adopted. Initial calculations showed that a symmetrical elastoplastic model would lead to overestimation of compressive forces in the steel because it

ignores the Bauschinger effect. Unit stresses (σ_s) associated with average unit strains (ε) were therefore estimated using a Ramberg-Osgood (1943) model:

Before the first reversal in the inelastic range of response:

$$|\sigma_s| = E_s \cdot |\varepsilon| \text{ for } |\varepsilon| < \frac{f_y}{E_s}$$
 (2.9-1)

$$|\sigma_s| = f_y + m \cdot E_s \cdot \left(|\varepsilon| - \frac{f_y}{E_s} \right) \text{ for } |\varepsilon| \ge \frac{f_y}{E_s}$$
 (2.9-2)

For subsequent half cycles:

$$\frac{\left|\varepsilon - \varepsilon_{i}\right|}{\frac{\sigma_{o}}{E_{s}}} = \frac{\left|\sigma_{s} - \sigma_{i}\right|}{\sigma_{o}} + \left(\frac{\left|\sigma_{s} - \sigma_{i}\right|}{\sigma_{o}}\right)^{\alpha} \tag{2.9-3}$$

where

$$\sigma_o = 47,000 + 0.5 \cdot (\sigma_{max} - \sigma_{min})$$
 (2.9-4)

and α is such that

$$\sigma_s = \frac{-\sigma_i}{|\sigma_i|} \cdot 110,000 \, psi \text{ for } \varepsilon = \varepsilon_i + \frac{-\sigma_i}{|\sigma_i|} \cdot 0.09$$
 (2.9-5)

Positive signs refer to tensile unit stresses and strains. The initial unit stress σ_i and unit strain ε_i for a given half cycle are defined in Figure 2.9-1.

The unit stresses σ_{max} and σ_{min} are the maximum and minimum unit stresses (considering the signs) reached during half cycles before the half cycle considered.

The parameters used for describing the response of the steel before the first reversal reflect the mechanical properties measured for the ³/₄-in. bars (see the Appendix):

 $f_{\rm V} = 65.7 \; {\rm ksi.}$ (Unit yield stress)

 $E_s = 29,000 \text{ ksi}$ (Initial modulus of Elasticity)

m = 0.02 (Ratio of the average slope of the unit stress-unit strain curve after yielding to E_s)

The other parameters were chosen by rounding values obtained by Aktan (1973) for a particular set of No. 6 and No. 9 bars.

Using the unit stresses calculated with the unit stress-unit strain relationship described and nominal cross sectional areas, the forces in the steel bars were calculated for selected test stages. The history of the compressive force required to balance the applied axial force and the calculated forces in the steel is shown in Figures 2.9-2 to 2.9-9 for all test specimens. The values obtained are plausible but no clear trends are observed. For some specimens the average force in the concrete seemed to change with increasing number of applied cycles. The rate of this change was not consistent for similar specimens and it was observed to be very sensitive to variation of the parameters assumed to describe the response of the steel to cyclic loads.

2.10 Comparisons: Effect of Independent Variables

Figures 2.10-1 to 2.10-3 show comparisons of the initial response of different specimens, classified according to axial load level and initial drift ratio target. The responses compared are consistent, indicating that other variables did not have a perceptible effect on the initial response of the specimens.

The ranges of the controlled variables were:

Hoop Spacing (Transverse reinforcement ratio): 1.5 - 3 in. (1.1% - 0.6%),

Axial Load: $30 - 60 \text{ kips } (0.08 - 0.21 \cdot f'_c \cdot A_g),$

Maximum Drift Ratio: 1% - 4%,

Displacement History: See Table 2.1-1,

where f'_c is the compressive strength of the concrete and A_g is the gross cross-sectional area.

All these variables affect the drift capacity of a column. Hoops control the width of inclined cracks, provide confinement to the concrete core, and help reduce the magnitude of shear stresses acting on the concrete. Axial load has a dual role because it causes an increase in the monotonic shear strength of concrete members, but its presence is also associated with higher flexural strength, and therefore, higher maximum possible shear stresses. The main variable in the tests was the displacement history. Two series of

experiments with similar specimens (specimens 10-2-3 and 10-3-3, and specimens 10-1-2¹/₄, 10-2-2¹/₄, and 10-3-2¹/₄) tested under different displacement schedules were carried out to study whether displacement history has an effect on drift capacity. The observed effects for each of these variables are described next.

2.10.1 Hoop Spacing

The effect of hoop spacing on the response of the specimens during their complete load histories can be inferred from Figures 2.10.1-1 and 2.10.1-2. Figure 2.10.1-1 shows the variation of stiffness with number of cycles to a drift ratio of 3% for specimens 10-2-2½ North and 10-2-3 North. Both specimens were tested under 30 kips of axial load and both were subjected to 7 displacement cycles at a maximum drift ratio of 2% before being displaced to a drift ratio of 3%. But the hoops in specimen 10-2-2½ North were placed every 2½ inches, while the hoops in specimen 10-2-3 North were placed every 3 inches. Specimens 10-2-2½ showed a less rapid reduction in stiffness with cycles of displacement. Similarly, the stiffness histories shown in Figure 2.10.1-2 correspond to specimens tested under the same displacement schedule and axial load but with different amounts of transverse reinforcement (specimens 10-3-3 North and 10-3-2½ North). The hoops in specimen 10-3-3 North were spaced at 3 in. and the hoops in specimen 10-3-2½ North were spaced at 2½ in. Again, the smaller the hoop spacing, the larger was the number of cycles that could be sustained before stiffness reduction at a given maximum drift ratio.

As discussed before, the overall displacement response of a specimen was observed to be related to the magnitude of transverse deformations measured in the plastic hinge region. The effect of hoop spacing on the history of transverse deformations can be inferred by comparing Figures 2.5-1 and 2.5-13. The transverse strains in the specimen with less transverse reinforcement (10-2-3 North) increased faster than in the specimen with more hoops (10-2-2½ North). The same trend is observed when comparing the histories of transverse deformations for specimens 10-3-3 North and 10-3-2½ North (Figures 2.5-5 and 2.5-7).

2.10.2 Axial Load

The responses of specimens 10-3-3 North and 20-3-3 South are compared in Figure 2.10.2-1. The spacing of the hoops in both specimens was 3 in. Both specimens were tested under displacement cycles to a drift ratio of 3%. But specimen 20-3-3 South was tested under a 60-kip axial load ($0.16\ f'_c\cdot A_g$) while the axial load applied to specimen 10-3-3 North was 30 kips ($0.10\ f'_c\cdot A_g$). The rate at which stiffness decreased for the initial displacement cycles was larger for the specimen with the lower axial load (10-3-3 North). Transverse strains also were observed to increase more rapidly with initial displacement cycles for specimen 10-3-3 North (Figures 2.5-5 and 2.5-12). The total stiffness decrease exceeded 20 % of the initial stiffness during cycle 8 for specimen 20-3-3 South and cycle 7 for specimen 10-3-3 North (Table 2.4-1). But the rate at which stiffness decreased during the final displacement cycles was much higher for the specimen with the higher axial load (20-3-3 South). The higher the axial load, the more abrupt was the failure process.

The responses of specimens $10\text{-}3\text{-}1\frac{1}{2}$ South and $20\text{-}3\text{-}1\frac{1}{2}$ North are compared in Figure 2.10.2-2. The variation of stiffness with number of cycles shown for specimen $20\text{-}3\text{-}1\frac{1}{2}$ North is limited to cycles applied before buckling of the longitudinal reinforcement at the joint face. The spacing of the hoops in both specimens was $1\frac{1}{2}$ in. Both specimens were tested under displacement cycles at a drift ratio of 4% after 7 cycles at a drift ratio of 3%. Specimen $20\text{-}3\text{-}1\frac{1}{2}$ North was tested under a 60-kip axial load $(0.21\ f'_{\ C}\cdot A_g)$ while the axial load applied to specimen $10\text{-}3\text{-}1\frac{1}{2}$ South was $30\ \text{kips}$ ($0.09\ f'_{\ C}\cdot A_g$). The rate at which stiffness decreased for the initial displacement cycles applied to both specimens was similar despite the fact transverse deformations increased more rapidly for the specimen with the lower axial load (Figures 2.5-4 and 2.5-9). A total stiffness decrease of 20% of the initial stiffness value or more did not take place earlier in the specimen with the higher axial load ($20\text{-}3\text{-}1\frac{1}{2}$ North).

The higher axial load did not affect significantly the number of cycles that could be sustained by a column at a given drift ratio. But axial load did affect the rate at which stiffness decreased during the final displacement cycles. The higher the axial load, the more abrupt was the failure process.

2.10.3 Displacement History

This series of tests indicated categorically that the displacement history affected response under cyclic loading. The number of cycles that can be sustained at a given maximum drift ratio decreased with increasing number and amplitude of previous cycles in the inelastic range of response. Cycles before yielding of the longitudinal reinforcement did not affect the response at higher amplitude cycles.

Two series of experiments with similar specimens (specimens 10-2-3 and 10-3-3, and specimens 10-1-21/4, 10-2-21/4, and 10-3-21/4) tested under different displacement schedules were carried out to study whether displacement history has an effect on drift capacity.

Specimens 10-1-2¼, 10-2-2¼, and 10-3-2¼ were subjected to the same axial load (30 kips) and had the same reinforcement details (2¼ in. hoop spacing). All three sets of specimens were tested at a drift ratio of 3%. Specimens 10-3-2¼ were displaced directly to a drift ratio of 3%. Specimens 10-1-2¼ were subjected to seven cycles at a drift ratio of 1% (approximately the drift ratio at yield) and specimens 10-2-2¼ were subjected to seven cycles at a drift ratio of 2% before application of cycles at 3%. The responses recorded for the specimens that failed in these assemblies are shown in Figure 2.10.3-1. It can be seen that the damage caused by cycles at a drift ratio of 2% affected the response at 3%. On the other hand, damage caused by cycles at 1% did not accelerate the loss of stiffness with cycles at 3%. Stiffness loss during the final cycles applied to specimen 10-3-2 ¼ North occurred at a rate that was even higher than the final rate of stiffness decay for specimen 10-1-2¼ South. This may be due to the lower strength of the concrete in specimens 10-3-2 ¼ (Table A.2.1-2).

Similarly, specimens 10-2-3 and 10-3-3 had the same axial load (30 kips) and the same amount of transverse reinforcement (3-in. hoop spacing) but were tested under different displacement histories. Specimens 10-2-3 were subjected to 7 cycles at a drift ratio of 2% before being tested at 3%. On the other hand, specimens 10-3-3 were tested directly at 3%. Again, the damage produced by cycles at 2% drift ratio caused the stiffness decrease with cycles at 3% to accelerate (Figure 2.10.3-2).

The recorded histories of transverse deformations show trends that are consistent with the observed variations in stiffness. Comparison of Figures 2.5-7 and 2.5-13 shows that cycles at a drift ratio of 3% caused a more rapid increase in transverse strain for specimen 10-2-2½ North (subjected to 7 initial cycles at 2%) than in specimen 10-3-2½ North (tested only at 3%). In contrast, the rate at which transverse strains increased during cycles at a drift ratio of 3% was similar for specimens 10-3-2½ North (Figure 2.5-7) and 10-1-2½ South (subjected to 7 initial cycles at 1%; Figure 2.5-16). In fact, the cycles at a drift ratio of 1% applied to specimen 10-1-2½ South did not cause continuous accumulation of transverse strains with increasing number of cycles. In all cases, cycles at larger drift ratios caused continuous accumulation of transverse strains.

3 DISPLACEMENT COMPONENTS

3.1 Introduction

As discussed in Section 2.5, the overall behavior and the magnitude of changes in the dimensions of the test specimens were observed to be related. In an attempt to understand how stiffness varied with specific changes in the geometry of the specimens, a study of the history of the deformations caused by the applied loads was conducted. This study is presented in Section 3.2.

Changes in the geometry of the test specimens were measured using Whittemore gages as described in detail in the Appendix. The locations of the gage stations are shown in Figure A.4.2-5. Each gage station comprised four reference points that formed a square on the concrete surface. These squares were numbered from the center stub out and they will be referred to as "gage locations" (Figure 2.1-2).

3.2 Calculation of Displacement Components

In each gage location, six measurements were made: one on each side of the square and two diagonal measurements (Figure A.4.2-5). The distance between two reference points at a given test stage was calculated as the sum of the nominal distance between them and the measured change in distance. Knowing the distances between reference points allowed calculation of the relative coordinates for all reference points by triangulation. The segment of each specimen that was not instrumented was assumed not to contribute to drift.

Deflection components were calculated based on calculated angular changes in the Whittemore reference mesh. Figure 3.2-1 shows a gage location at a given test stage. As illustrated in this figure, it was assumed that the change in any angle of the square has three components:

- 1) Angular change related to bending
- 2) Angular change related to shear distortion
- 3) Angular change related to expansion of the concrete core near the base of the column.

The average rotation (θ) at a gage location was estimated from angular changes calculated as follows, (see Figure 3.2-1 for definitions):

$$\Delta A = A - \frac{\pi}{4} = \frac{\theta}{2} + \nu + \psi \tag{3.2-1}$$

$$\Delta B = B - \frac{\pi}{4} = \frac{\theta}{2} - v - \psi \tag{3.2-2}$$

$$\Delta C = C - \frac{\pi}{4} = \frac{-\theta}{2} + \nu - \psi \tag{3.2-3}$$

$$\Delta D = D - \frac{\pi}{4} = \frac{-\theta}{2} - \nu + \psi \tag{3.2-4}$$

$$\Delta A + \Delta B - \Delta C - \Delta D = \left(\frac{\theta}{2} + v + \psi\right) + \left(\frac{\theta}{2} - v - \psi\right) - \left(\frac{-\theta}{2} + v - \psi\right)$$
$$-\left(\frac{-\theta}{2} - v + \psi\right) = 2\theta \tag{3.2-5}$$

Calculation of rotation as the ratio of the difference between the two horizontal measurements to the nominal height of the gage location (8 in.) yielded the same results.

Angles A, B, C and D were calculated using the cosine law and the calculated distances between reference points (see Figure 3.2-1 for definitions):

$$A = a\cos\left[\frac{(h_t)^2 + (v_l)^2 - (d_2)^2}{2 \cdot h_t \cdot v_l}\right]$$
(3.2-6)

$$B = a\cos\left[\frac{(h_t)^2 + (v_r)^2 - (d_1)^2}{2 \cdot h_t \cdot v_r}\right]$$
(3.2-7)

$$C = a\cos\left[\frac{(h_b)^2 + (v_r)^2 - (d_2)^2}{2 \cdot h_b \cdot v_r}\right]$$
(3.2-8)

$$D = a\cos\left[\frac{(h_b)^2 + (v_l)^2 - (d_1)^2}{2 \cdot h_b \cdot v_l}\right]$$
(3.2-9)

The average distortion (ν) was calculated as follows:

$$\Delta A - \Delta B + \Delta C - \Delta D = \left(\frac{\theta}{2} + v + \psi\right) - \left(\frac{\theta}{2} - v - \psi\right) + \left(\frac{-\theta}{2} + v - \psi\right)$$
$$-\left(\frac{-\theta}{2} - v + \psi\right) = 2\theta \tag{3.2-10}$$

Observe that angular changes due to expansion of the concrete core always cancel out.

It was assumed that there are two deflection components. The first component (Δ_b) is related to bending deformations and slip of the reinforcement in the joint (Figure 3.2-2). The contribution from a gage location (i) to this component was calculated as the product of its average rotation (θ_i) times its nominal distance to the support. The total deflection at the joint face due to bending and slip (Δ_b) was calculated as follows:

$$\Delta_b = \int_{i=1}^{3} \theta_i \cdot [31in - (i-1) \cdot 8in] - \theta_1 \cdot 4in$$
 (3.2-11)

The second deflection component (Δ_{shear}) is related to shear distortion (Figure 3.2-2). The contribution from a gage location (i) to this component was calculated as the product of its average shear distortion (v_i) times its nominal horizontal dimension (8 in.). The total deflection at the joint face due to shear distortion was calculated as the sum of the contributions from gage locations 2 and 3:

$$\Delta_{shear} = \begin{cases} 3 \\ v_i \cdot 8in \end{cases}$$
 (3.2-12)

Again, the segment of each specimen that was not instrumented was assumed not to contribute to drift. Total deflection was calculated as the sum of Δ_b and Δ_{shear} and it matched very well the deflection calculated by triangulating.

Figures 3.2-3 to 3.2-18 show the variation of the calculated drift ratio (ratio of total displacement to shear span) for all the tests. Measured drift ratios are also shown for comparison. Positive values correspond to downward deflections. The match between calculated and measured drift ratios is very good.

Figures 3.2-19 to 3.2-34 show the variation of the calculated drift ratio components through the tests. It can be seen that deflections due to shear increase with increasing number of cycles and cycle amplitude. On the other hand, deflections due to flexure decrease with increasing number of cycles. Because of the loss of Whittemore reference points caused by crushing of the concrete, some of these plots lack results from the last load cycles. Usually, crushing of concrete affected the points near the joint face first. In the next section, a study of the history of the deformation components within each gage location is presented. Treating each gage location separately allows visualization of additional data from locations away from the center stub, where reference points remained glued to the concrete for a larger number of cycles.

3.3 Displacement Components vs. Number of Cycles

Figures 3.3-1 to 3.3-32 show the history of calculated values of angular change due to bending (θ) , and shear (v) for gage locations 2 and 3. Gage location 2 is formed by points at the joint face and points at 8 in. from the joint face. Gage location 3 is formed by points at 8 and 16 in. from the joint face (Figure 2.1-2). Angular change is defined in Figure 3.2-1. Positive values of rotation indicate compression at the top and tension at the bottom of the specimen. Positive values of shear distortion correspond to downward deflections. As expected, values of angular change are larger for location 2.

There are two trends that are common to all the measurements: shear angular distortion increases while flexural angular change decreases with increasing number of displacement cycles at drift ratios exceeding 1%. This implies that the decrease in the stiffness of the specimens observed through the tests was related to a decrease in shear stiffness. Because this process and the continuous increase in transverse deformations took place simultaneously, it is reasonable to assume that they are related. It seems plausible that, as confinement was lost due to the continuous stretching of the hoops, more movement of the particles in the collection of concrete fragments defined by inclined cracks was required to reach the same level of friction between particles (Figure 3.3-33).

3.4 Theoretical Displacement Components

To gain insight about the relative magnitude of the displacements measured, they were compared with displacements calculated using conventional analytical methods. This comparison was limited to displacements reached before the first displacement reversal.

Displacements were calculated assuming the total displacement of a column to have three components. The first component is related to bending (Δ_f). The second component is related to slip of the reinforcement and deformations of the base of the column (Δ_{slip}). The third component is related to shear deformations (Δ_{shear}).

The displacement component related to bending was calculated as the first moment with respect to the support point of the area under a diagram representing the distribution of curvature along the column. The curvature distribution before yielding of the longitudinal reinforcement was estimated from equilibrium and moment-curvature diagrams (Figure 3.4-1) calculated assuming linear distribution of strains and the stress-strain relationships shown in Figures 3.4-2 and 3.4-3. After yielding, additional rotations were assumed to be proportional to the effective depth (d) and to concentrate at the face of the base of the column:

$$\Delta_f = (\phi_p - \phi_y) \cdot d \cdot a + \Delta_y \tag{3.4-1}$$

where

 ϕ_p : curvature after yield,

 ϕ_{V} : curvature at yield,

a : shear span,

 $\Delta_{\rm v}$: yield displacement.

The displacement component related to slip of the reinforcement under tensile forces was calculated assuming the stresses in the steel in the base to vary linearly:

$$f_o = f_s - \frac{4 \cdot l}{d_b} \mu \ge 0 \tag{3.4-2}$$

Here

 f_o : tensile unit stress at the center of the joint,

 f_s : tensile unit stress at the face of the joint,

l : half of the length of the center stub (9 in.),

 d_b : diameter of the longitudinal bars (3/4 in.),

 μ : average bond stress.

The distribution of unit strains corresponding to the assumed distribution of unit stresses was obtained using the relationship in Figure 3.4-2. Slip was then calculated as the integral of the calculated strain distribution along half of center stub (Figure 3.4-4).

The reverse of this process was used to estimate average bond stresses from data from strain gages installed on the longitudinal bars at the center of the joint and at the joint face. Unit strains were converted into unit stresses using the relationship shown in Figure 3.4-2. Average bond stresses were then calculated using the expression:

$$\mu = (f_s - f_o) \cdot \frac{d_b}{4 \cdot l} \tag{3.4-3}$$

The calculated bond stresses are shown in Figure 3.4-5. Observe that, after yielding of the reinforcement, bond stresses remain constant for an ample range of

maximum strains, including strains larger than those observed in coupons at the beginning of strain hardening (Table A.2.2-1). Before yielding of the reinforcement, bond stresses increase with increasing magnitude of the force at the face of the center stub. The following expression was adopted for calculation of average bond stresses:

$$\mu = 4{,}300 \cdot (\varepsilon_s - \varepsilon_{ini}) \sqrt{f_c'} \le 4.5 \sqrt{f_c'} \tag{3.4-4}$$

In this expression

 \mathcal{E}_{S} : unit strain at the joint face,

 ε_{ini} : unit strain at the joint face for zero transverse load,

 f'_c : concrete compressive strength, in psi.

Calculation of the rotation related to slip requires estimation of the possible indentation of the concrete in the base under compressive forces. The indentation at the level of the reinforcement in compression was measured using an 8-in. Whittemore gage. The values measured at yield are shown in Table 3.4-1. The following expression was adopted for calculation of average indentation values:

$$ind = 0.00021 \frac{in}{kip} \cdot V \quad \text{for } V \le 24kips \tag{3.4-5}$$

$$ind = 0.005in + 0.001 \frac{in}{kip} \cdot (V - 24kips)$$
 for $V > 24kips$ (3.4-6)

The total rotation related to slip and deformation of the base was calculated as the ratio of the sum of the slip and the indentation to the distance between the two layers of longitudinal reinforcement ($d - d_c$):

$$\theta_{slip} = \frac{slip + ind}{d - d_c} \tag{3.4-7}$$

Therefore:

$$\Delta_{slip} = \theta_{slip} \cdot a = \frac{slip + ind}{d - d_c} \cdot a \tag{3.4-8}$$

where

a: shear span,

d: effective depth,

 d_c : h - d, where h is the cross-sectional depth.

Calculation of the displacement component related to shear before cracking can be made using the expression from mechanics of materials:

$$\Delta_{shear} = \frac{6}{5} \cdot \frac{V}{b \cdot h \cdot G} \cdot a \tag{3.4-9}$$

where

V : shear force,

G: shear modulus of the concrete (estimated as 0.4 times the modulus of

elasticity),

h : cross-sectional depth,

b : cross-sectional width,

a: shear span.

As shown in Figure 3.4-6, this expression yields results that are smaller than the shear displacements calculated from Whittemore readings. Based on these readings, the following expression was adopted for estimation of displacements related to shear:

$$\Delta_{shear} = 0.15 \cdot \left(\Delta_f + \Delta_{slip} \right) \tag{3.4-10}$$

Figures 3.4-7 to 3.4-9 show the calculated history of drift ratio (ratio of total displacement to shear span) compared with the drift ratio history recorded during the first half load cycle. When studying this comparison one has to keep in mind that displacement components Δ_{slip} and Δ_{shear} were calibrated based on deformation

measurements. The match is acceptable but, as observed in previous investigations (Konwinski 1996, Yamashiro 1962), the deflections measured are consistently larger than the displacements calculated for loads larger than those at cracking of the concrete.

4 TWO MODELS

4.1 Introduction

Two observations have been discussed in previous chapters:

- 1) Stiffness decreased with increasing number of displacement cycles in the inelastic range of response.
- 2) The decrease in stiffness exceeded 20% after transverse unit strains exceeded 3%.

The observed variation of transverse deformation with number of cycles is discussed Section 4.2. If this relationship can be determined on the basis of material and geometric properties of the column, the cycle at which a drop in stiffness of 20% is likely to occur can be estimated as the cycle during which a unit transverse strain of 3% is reached.

4.2 Transverse Deformations

As shown in Figures 2.5-1 to 2.5-16, transverse deformations increased with increasing number of cycles at drift ratios exceeding 1%. Figure 4.2-1 shows a typical variation of transverse strain with drift ratio. In each load cycle, transverse deformations increased during loading and decreased during unloading but the decrease was less than the increase. There was permanent deformation in each half cycle. An idealization of this relationship is shown in Figure 4.2-2. In this model, the increase in transverse deformations related to loading in either direction is assumed constant for cycles of constant amplitude. After the first unloading, cracks remain open. Initial crack widths and transverse deformations are proportional to the magnitude of permanent member displacements. Assuming that this approximate proportionality is also valid for subsequent cycles with the same amplitude:

$$\frac{\delta_r}{\delta_{max}} = \frac{\gamma_r}{\gamma_{max}} \tag{4.2-1}$$

 δ_r : decrease in transverse deformation related to unloading during a given cycle,

 γ_{max} : maximum drift ratio reached during a cycle,

 δ_{max} : increase in transverse deformation related to loading up to a maximum drift ratio equal to γ_{max} ,

 γ_r : decrease in drift ratio related to unloading from γ_{max} .

Given this relationship, the history of transverse deformations can be expressed mathematically as a function of δ_{max} , which, in turn, was observed (Figures 2.5-1 to 2.5-16) to be a function of the cycle amplitude and the amount the transverse reinforcement. Two models to estimate δ_{max} are discussed in the following sections.

4.3 Model A

In model A, transverse deformation is assumed to increase linearly with increasing drift ratio after yielding of the longitudinal reinforcement. Transverse deformation at yield of the longitudinal reinforcement is assumed proportional to the force in the transverse reinforcement crossing an inclined crack near the joint, V_s , which is, in turn, assumed to be a fraction of the total shear at yield, V_{yield} :

$$V_s = V_{yield} - V_c \ge 0 \tag{4.3-1}$$

where V_c is the shear force assumed to be carried by the concrete. The force V_c is estimated, following the format proposed by Olesen et al. (1967), as the summation of the shear force that causes flexural cracking at a distance d/2 from the joint and the product $b \cdot d \cdot \sqrt{f'_c}$:

$$V_c = b \cdot d \cdot \sqrt{f_c'} + \frac{M_{cr}}{a - \frac{d}{2}}$$

$$(4.3-2)$$

where

d : effective depth,

a: shear span,

b : cross-sectional width,

 f'_c : concrete compressive strength in psi,

 M_{cr} : moment at first cracking, approximated, for simplicity, using gross

section properties,

$$M_{cr} = \frac{I_g}{\frac{h}{2}} \cdot \left(f_{cr} + \frac{P}{A_g} \right) \tag{4.3-3}$$

P : axial load,

h : cross-sectional depth,

 I_g : is the moment of inertia of the gross cross-section,

 A_g : area of the gross cross-section,

 f_{cr} : modulus of rupture (taken as $12\sqrt{f_c'}$, f_c' in psi, on the basis of the

data shown in Figure A.2.1-13).

The shear force carried by a single hoop in the plastic hinge region is approximated as $V_s / (d/s)$, where d is the effective depth and s is the hoop spacing. The strain associated with this force is assumed to be distributed uniformly along the vertical legs of the hoop, whose length is approximated as the distance between exterior layers of longitudinal reinforcement $(d-d_c)$:

$$\delta_{yield} = (d - d_c) \cdot \frac{V_s \cdot s}{E_s \cdot A_w \cdot d}$$
 (4.3-4)

 E_s : steel modulus of elasticity,

 A_w : total cross-sectional area for a single hoop,

d : effective depth

 d_c : h-d, where h stands for cross-sectional depth.

Transverse deformations for drifts larger than the drift at yield are calculated using a linear projection:

$$\delta_{max} = \delta_{yield} \frac{\gamma}{\gamma_{yield}} \tag{4.3-5}$$

 δ_{vield} : transverse deformation at yield (defined earlier),

 γ : drift ratio,

 γ_{vield} : drift ratio at yield (taken as 1% for the tests described here).

Table 4.3-1 shows calculated values of δ_{yield} and values used for the model parameters.

4.4 Model B

Model A describes the initial variation of transverse deformations with increasing drift ratio based on a formulation that was developed originally for a strength criterion (Richart, 1927). The applicability of this formulation to the problem in hand can only be justified on the basis of experimental data. Moreover, the initial assumption of linear proportionality between shear forces and transverse deformation is ignored for drifts larger than the drift at yield. The fact that shear forces remain practically constant after yield is ignored and transverse strains are assumed to increase with increasing drift at the same rate they increase before yielding. Despite this contradiction, the model may still yield acceptable results. However, a more consistent model was believed desirable.

In Model B, all rotation is assumed to occur in two cracks: a vertical crack at the joint face and an inclined crack that forms an angle ϕ with the column axis equal to 45° (Figure 4.4-1). The total drift ratio is therefore assumed equal to the sum of the angles formed by the two lines that define each crack:

$$\gamma = \theta_1 + \theta_2 \tag{4.4-1}$$

The length of the transverse projection of the inclined crack, $\beta \cdot d \cdot tan(\phi)$, is assumed to be equal to the distance between exterior layers of longitudinal reinforcement $(d-d_c)$. For the dimensions of the specimens tested in this study, this assumption is equivalent to assuming $\beta = 0.8$. All transverse reinforcement crossing the inclined crack is assumed to have reached the yield unit stress (f_{yw}) by the time inelastic column displacements are reached and to be concentrated at a distance $0.5 \beta \cdot d$ from the joint face.

From equilibrium of moments with respect to the point where the two cracks meet (Figure 4.4-1):

$$(T_2 - T_1) \cdot \beta \cdot d \cdot tan(\phi) = f_{yw} \cdot \frac{A_w \cdot \beta \cdot d}{s} \cdot \frac{\beta \cdot d}{2}$$
 (4.4-2)

 T_2 : force in the longitudinal reinforcement in tension at its intersection with the vertical crack,

 T_1 : force in the longitudinal reinforcement in tension at its intersection with the inclined crack,

 A_{W} : total transverse reinforcement cross-sectional area,

s : hoop spacing.

If $\phi = 45^{\circ}$,

$$T_2 - T_1 = f_{yw} \cdot \frac{A_w \cdot \beta \cdot d}{2 \cdot s} \tag{4.4-3}$$

The unit strains ε_1 and ε_2 associated with forces T_1 and T_2 are expressed in terms of θ_1 and θ_2 using the following approximations (Figures 4.4-2 and 4.4-3):

$$\varepsilon_1 = \frac{\theta_1 \cdot \beta}{\alpha_1 \cdot \cos(\phi) \cdot \sin(\phi)} \tag{4.4-4}$$

$$\varepsilon_2 = \frac{\theta_2 \cdot \beta \cdot \tan(\phi)}{\alpha_2} \tag{4.4-5}$$

The relationship between unit strains and unit stresses used to relate ε_1 and ε_2 to T_1 and T_2 is shown in Figure 3.4-2.

Initial calculations indicated that taking $\alpha_1 = 3/4$ and $\alpha_2 = 1$ leads to reasonable estimates of initial unit strains in the longitudinal reinforcement (Figures 4.4-4 to 4.4-9). Using these values of α_1 and α_2 , and for $\phi = 45^\circ$:

$$\varepsilon_1 = \frac{8}{3} \cdot \theta_1 \cdot \beta \tag{4.4-6}$$

$$\varepsilon_2 = \theta_2 \cdot \beta \tag{4.4-7}$$

This formulation can therefore be reduced to a system of two variables, θ_1 and θ_2 , and two equations:

$$\gamma = \theta_1 + \theta_2 \tag{4.4-8}$$

$$T_2 - T_1 = f_{yw} \cdot \frac{A_w \cdot \beta \cdot d}{2 \cdot s} \tag{4.4-9}$$

Where T_1 and T_2 are functions of θ_1 and θ_2 , respectively. After solving this system of equations, the transverse deformation δ_{max} can be calculated using the expression (Figures 4.4-1 and 4.4-3):

$$\delta_{max} = \frac{\theta_1 \cdot \beta \cdot d}{2[\cos(\phi)]^2} = \theta_1 \cdot \beta \cdot d \tag{4.4-10}$$

Table 4.3-2 shows calculated values of δ_{max} , θ_1 , and θ_2 , for $\alpha_1 = 0.75$, $\alpha_2 = 1$, β =0.8 and several values of drift ratio, γ .

4.5 Results

Models A and B allow calculation of δ_{max} , the increase in transverse deformations caused by loading up to a drift ratio γ_{max} . The total unit transverse deformation (ε_t) after cycles with different amplitude is,

$$\varepsilon_{t} = \frac{1}{d - d_{c}} \int_{i=1}^{n} 2 \cdot \delta_{max \, i} \cdot \left(1 - \frac{\gamma_{r \, i}}{\gamma_{max \, i}} \right)$$
(4.5-1)

 $\delta_{max\ i}$: Increase in transverse deformation related to loading up to a drift ratio equal to $\gamma_{max\ i}$. It can be estimated on the basis of material and geometric properties of the column as shown in Sections 4.3 and 4.4.

 $\gamma_{max i}$: Maximum drift ratio reached during cycle *i*.

 γ_{ri} : Decrease in drift ratio related to unloading from γ_{maxi} .

n : Total number of cycles applied.

d : Effective depth

 d_c : h - d, where h stands for cross-sectional depth.

Figures 4.5-1 to 4.5-2 show the number of the cycle for which a transverse deformation of $\frac{1}{4}$ in (3% transverse unit strain) was calculated using measured values of $\frac{1}{4}$ compared with the cycle number for both, a measured decrease in stiffness of 20%, and a measured transverse deformation of $\frac{1}{4}$ in. The results from both models are very good but Model B, whose use requires more computational effort, leads to a slightly better match.

4.6 Comparison with Data from Previous Experiments

In Section 1.4, data from previous experiments of columns under displacement reversals were described. Those data were organized in terms of column drift capacity, the maximum drift reached before a reduction in strength of more than 20%, using a criterion proposed in the initial stages of this investigation (Pujol et al., 2000).

The drift capacity data from the previous tests considered were normalized with respect to the ratio of shear span to effective depth (a/d) and classified with respect to k_1 , a parameter that describes the strength of the concrete in the column core in terms of the concrete compressive strength. The parameter k_1 , defined in Figure 1.4-1, is assumed to decrease with cyclic displacements reversals.

The drift capacity data from the tests presented here can be organized in the same manner but a direct comparison cannot be made because the displacement schedules used in these experiments are very different from those used in previous investigations. In the experiments carried out as part of this study, the number of cycles applied per displacement increment was larger. If displacement-history effects are ignored, the drift ratios reached during the tests described here appear small when compared with results from the tests described in Section 1.4 (Figure 4.6-1). In order to project these data to the case of a displacement schedule with fewer cycles per displacement increment, the expression proposed in Section 4.5 for transverse deformations was simplified as follows:

$$\varepsilon_{t} = \frac{1}{d - d_{c}} \int_{i=1}^{n} 2 \cdot \delta_{max \, i} \cdot \left(1 - \frac{0.01}{\gamma_{max \, i}} \right), \, \gamma_{max \, i} \ge 0.01.$$
 (4.6-1)

This simplification is convenient because it implies that, as observed for this particular set of tests, cycles at a drift ratio of 1% do not cause accumulation of transverse strains. It is also a conservative approximation because decreases in drift ratio larger than 0.01 were observed during unloading (Figures 2.2-1 to 2.2-16) and the smaller the decrease in drift ratio assumed, the larger will be the estimated accumulation of transverse deformation. This expression and the values of δ_{max} calculated in Section 4.4. can be used to calculate the maximum drift that can be reached by a column similar to the ones tested for an assumed displacement schedule. The results obtained here were projected to the case of a displacement history with 2 cycles at a drift ratio of 1% followed by pairs of cycles at drift ratios increasing by increments of 1% (Figure 4.6-2). The maximum drift ratio for the cycle corresponding to a calculated transverse unit strain of 3% was taken as the projected column drift capacity.

Four cases were considered:

- 1½, 2¼ and 3-in. hoop spacing and a 30-kip axial load,
- and 3-in hoop spacing and a 60-kip axial load.

Other possible combinations of variables were not considered because they were either not included in the test program or they did not lead to the failure mode under study. The results obtained are compared with the data described in Chapter 1 in Figure 4.6-3. When projected as described, the results from the tests presented here seem to follow the same general trend as the data from previous experiments.

4.7 Number of Cycles for Recorded Ground Motions

Ingham et al. (2001) suggested that standard laboratory displacement histories are more demanding than displacement histories projected from recorded ground acceleration histories for regular building structures. In fact, buildings are usually proportioned so that maximum calculated inter-story drift ratios for design ground motions remain under 2%. If inelastic displacement cycles affect the response of a given column, the number and amplitude of the cycles that a column in a regular reinforced concrete building frame may undergo during an earthquake needs to be estimated. A simple model was adopted here to estimate the response of a typical building frame during an earthquake. The responses of nonlinear single degree of freedom systems (SDOF) were used as reference. The stiffness, k, assumed for the SDOF systems modeled is given by the following expression (Figure 4.7-1):

$$k = \frac{1}{1 + c_1 \cdot r \cdot \left(\frac{|F|}{F_y}\right)^{r-1}} \cdot \frac{F_y}{\Delta_y} \quad \text{if } (\Delta x \cdot F) \ge 0$$

$$\frac{F_y}{\Delta_y} \quad \text{otherwise}$$
(4.7-1)

where

 F_{ν} : yield force,

 $\Delta_{\rm v}$: yield displacement,

F : force that "the spring" exerts on "the mass" of the SDOF system,

 Δx : displacement change caused by the input ground acceleration at a given point in time.

The parameters c_1 and r define the post-yield stiffness and the transition from the elastic range to the inelastic range of response. The values used were 0.3 and 7 for c_1 and r, respectively.

Three different reference oscillators were considered. Selected initial natural vibration periods included 1, 2 and 3 sec. The base shear strength of the oscillators was assumed to be 15% of the weight of the system. A constant damping factor of 2% of the critical damping was assumed. Displacement histories for the selected SDOF systems were calculated using Newmark's beta method with a beta factor of 0.25. The responses of the selected oscillators were then used to estimate the response of regular building frames based on the following assumptions:

- 1) The initial vibration period (in seconds) of a regular reinforced concrete building frame is equal to the number of stories divided by 10.
- 2) The typical story height is 10 ft.
- 3) The roof displacement is equal to 5/4 times the relative displacement for a SDOF with the same initial vibration period.
- 4) The maximum inter-story drift ratio (MIDR) is equal to 1.5 times the roof drift ratio, calculated as the ratio of total roof displacement to building height (Lepage, 1996).

Seven ground motion records were considered (Viña del Mar - Chile 1985; Tokachi-Oki - Japan, 1968; Bucharest - Romania, 1974; Duzce - Turkey, Nov. 1999; Corralitos - Loma Prieta, 1989; El Centro - Imperial Valley, 1940; Secretaría de Comunicaciones y Transporte - Mexico, 1985). All records were scaled to a peak ground acceleration of 0.4g. Tables 4.7-1 to 4.7-3 show the number of displacement waveform peaks that exceeded a drift ratio of 1 and 2% for the first six records. Results for the record from Mexico will be discussed separately. Observe that the calculated number of excursions beyond a drift ratio of 2% is small (3 was the maximum) in comparison to the number of excursions at similar and larger levels of drift included in the displacement histories used in this an previous investigations of columns under cyclic loads.

Consider the EW component of the El Centro record (Figure 4.7-2). This record is a common reference in earthquake engineering (Blume et al., 1961; Lepage 1996). Figures 4.7-3 to 4.7-5 show the responses of the idealized building frames described to the scaled version of the El Centro record. Observe that the number of cycles increases but their amplitudes decrease with decreasing initial period. In fact, not even for the most flexible of the frames analyzed the maximum drift ratio reached during a given cycle was larger than 2%. The expression in section 4.6 for transverse deformations can be used to show that, with a minimum amount of transverse reinforcement (hoop spacing equal to one fourth of the effective depth d – ACI 318 – or 0.67% transverse reinforcement ratio 1), a reinforced concrete member similar to the ones tested in this investigation can sustain more than 30 cycles at a drift ratio of 2% (δ_{max} = 0.008 in., calculated with Method B) or 7 cycles at a drift ratio of 3% (δ_{max} = 0.027 in., Method B).

The frequency content and the duration of the records considered do not represent the worst observed scenario in terms of associated number and amplitude of displacement cycles. Such a scenario may be better represented by a ground motion record similar to the one obtained at Secretaría de Comunicaciones y Transporte, Mexico City, during the 1985 Mexico earthquake (Figure 4.7-6). In this case, the properties of the soil in the region were such that the resulting ground motion had a very long duration and was characterized by waves with large periods and amplitude. The responses of the structures described to the Mexico record scaled to 0.4g peak ground acceleration are shown in Figures 4.7-7 to 4.7-9 for the time interval where the ground motion was stronger. The maximum drift ratios reached are very large and they could compromise the stability of the structures modeled. It is clear that the result in hand corresponds to an extreme case. In fact, the peak ground acceleration recorded for the original record obtained in Mexico was 0.17g. The large drifts calculated are a result of the scale factor used. But even in this extreme case, the total amplitude (absolute difference in the drift ratio for adjacent peaks) of most of the cycles is of the order of 1% to 2%. Only 4 to 5 cycles have

¹ Ratio of cross-sectional area of transverse reinforcement to the product of cross-sectional width times hoop spacing.

significantly larger amplitudes. The maximum total amplitude was of the order of 6% and the maximum drift ratio was of the order of 4%. Observe that the calculated load histories were not symmetric with respect to the time axis while the displacement schedules studied in this investigation were symmetric. A direct comparison cannot be made. From the data recorded in the experiments, it cannot be inferred directly whether displacement reversals from a drift ratio of -3% to a drift ratio of 3% would cause as much damage as displacement reversals from a drift ratio of -2% to a drift ratio of 4%. It is reasonable to assume, however, that displacement reversals from -4% to 4% would cause more damage than the latter. From the formulation presented in Section 4.6, a reinforced concrete member similar to the ones tested and with a hoop spacing of d/4 (0.67% transverse reinforcement ratio) would be able to sustain at least 4 cycles at a drift ratio of 4% ($\delta_{max} = 0.049$ in., calculated with Method B).

Elements of buildings with an irregular distribution of lateral stiffness along their height may undergo reversals at displacement levels larger than those for elements in regular buildings. Consider the nine-story frame model tested by Moehle (1980) (Figure 4.7-10). Observe that the height of the first story is twice the height of the other stories. Deformations caused by simulated ground motions concentrated at this level. The base shear strength of the model was approximately 30% of its weight. Figure 4.7-11 shows the measured first-story drift-ratio response to base accelerations modeled after the NS component of the El Centro 1940 record, scaled to 0.4g peak ground acceleration and after compressing the time scale by a factor of 2.5. Observe that only two to three cycles have total amplitudes larger than 2% and the maximum drift ratio measured is of the order of 2%. The initial vibration period of the model, measured during free-vibration tests before earthquake simulation, was 0.25 sec. Considering the scale factor used to model the base accelerations, the model represented a structure with a 0.6-sec. initial period. The vibration period of the model after the earthquake simulation was twice the initial period.

If, as indicated by the experimental data, cycles with total amplitudes of approximately 2% do not cause accumulation of transverse deformations, it can be concluded that, in the domains considered, displacement-history effects are not likely to

dominate the response of members of regular reinforced concrete frames with amounts of transverse reinforcement within the ranges recommended in current design guidelines (Pujol et al., 2000).

5 SUMMARY AND CONCLUSIONS

5.1 Summary

5.1.1 Objective and Scope

The objective of this study was to determine whether the displacement history has an effect on the drift capacity of reinforced concrete columns under inelastic displacement reversals. This study and its results are limited to cases satisfying the following conditions:

- 1) Drift cycles occur primarily in the plane defined by one of the principal axes of the cross section.
- 2) The drift capacity is not less than the drift at yield.
- 3) The maximum shear exceeds the shear at inclined cracking.
- 4) The "static" shear capacity is not less than the shear at yield.
- 5) The column core is effectively confined by transverse reinforcement.
- 6) Longitudinal reinforcement is restrained against buckling by transverse reinforcement.

The variables considered were:

Maximum nominal unit shear stress $V/(b d \sqrt{f_c'})$: 6 to 8 (stresses in psi)

Maximum core unit shear stress, $V/(A_c \sqrt{f_c'})$: 10 to 13 (stresses in psi)

Axial load (kept constant in each test), P: 0.08 to 0.21 f_c A_g (30-60 kips)

Transverse reinforcement ratio, $A_w/(b s)$: 0.6% to 1.1%

Nominal unit transverse stress, $A_w f_{yw}/(b_c s)$: 500 to 1000 psi

Maximum drift ratio, y_{max} : 3%-4%

The constants were as follows:

Concrete compressive strength, f_c : 4.1 to 5.2 ksi

Longitudinal reinforcement unit yield stress, f_v : 65.7 ksi

Longitudinal reinforcement ratio, ρ : 2.4%

Ratio of shear span a, to effective depth d: 2.7

Ratio of gross cross-sectional area A_g , to core area A_c : 2.0

V : maximum shear force,

b : cross-sectional width,

d: effective depth,

 A_W : total cross-sectional area in a layer of transverse reinforcement,

 f_{yw} : transverse reinforcement unit yield stress,

 b_c : concrete core cross-sectional width (measured center-to-center of

exterior transverse reinforcement),

 A_c : concrete core cross-sectional area (measured center-to-center of

exterior transverse reinforcement),

s : hoop spacing.

5.1.2 Previous Investigations

There is limited data on displacement-history effects for columns whose response may be dominated by shear. Probably for this reason, current analytical models (Aoyama, 1993; Moehle et al. 2000, Priestley et al. 1994; FEMA 273, 1997; Aschheim, 2000) do not consider displacement history as a variable.

5.1.3 Experimental Program

5.1.3.1 Test Specimens

The experimental program included eight test assemblies. An assembly consisted of two cantilever columns joined by a center stub through which cyclic transverse load was applied. The ranges of the variables in the experiments are summarized in Section 5.1.1. The variables controlled in the experiments were the spacing of the hoops outside the center stub, the axial load (kept constant in each test), and the displacement schedule.

<u>5.1.3.2 Response</u>

Inclined cracks were observed in all specimens before yielding of the longitudinal reinforcement. All specimens reached their full flexural capacity and inelastic deformations.

Cycles at maximum drift ratios exceeding 1% (which is approximately the yield drift ratio for the specimens tested) caused continuous widening of inclined cracks and, consequently, a permanent increase in the depth of cross sections within a distance equal to the effective depth from the joint face. The rate at which sections near the column base expanded increased with additional displacement cycles at a given drift ratio. This rate was observed to be a function of the axial load, the amount of transverse reinforcement, and the displacement history. Stiffness decrease and progressive damage of the concrete shell and core were also observed. The larger the maximum drift ratio, the faster were the disintegration and expansion of the concrete. Stiffness decrease and damage accelerated during the last displacement cycles.

A stiffness reduction of more than 20% was consistently measured only after transverse unit strains exceeding 3% were observed. This observation permits relating the overall response of a specimen under a given displacement schedule to a single simple variable that can be measured easily.

5.1.3.3 Effect of Independent Variables

The spacing of the hoops was observed to affect the displacement response of the test specimens significantly. The smaller the hoop spacing, the larger was the number of cycles that could be sustained at a given maximum drift ratio before stiffness reduction.

The axial load did not affect significantly the number of cycles that could be sustained at a given drift ratio before stiffness reduction. But axial load did affect the rate at which stiffness decreased during the final displacement cycles. The higher the axial load, the more abrupt was the failure process.

This series of tests indicated categorically that the displacement history affected the response of reinforced concrete columns under cyclic loading. The number of cycles that could be sustained at a given maximum drift ratio before a large reduction in stiffness decreased with increasing number and amplitude of previous displacement cycles in the inelastic range of response.

5.1.4 Displacement Components

Measured displacement components related to shear were observed to increase while displacement components related to flexure were observed to decrease with increasing number of cycles with maximum drift ratios larger than 1%. This implies that the reduction in column stiffness observed through the tests is related to a decrease in shear stiffness. This process and the continuous stretching of the transverse reinforcement observed near the column base seem to be related.

Deflections measured during first loading are consistently larger than those calculated using conventional analytical models. Measured displacement components related to shear were of the order of 15% of measured displacements related to bending and slip of the longitudinal reinforcement.

5.1.5 Models

Column stiffness decreases with increasing number of cycles at drift ratios exceeding the drift ratio at yield. The reduction in stiffness exceeds 20% after transverse unit strains exceed 3%. Within the realm of the variables described in Section 5.1.1, the maximum transverse unit strain can be estimated using Equation (4.5-1).

5.1.6 Number of Cycles for Recorded Ground Motions

The responses of models of buildings subjected to base accelerations simulated based on records scaled to a peak ground acceleration of 0.4g and the observations made in the experiments described herein indicate that displacement-history effects are not likely to dominate the response of members of regular reinforced concrete frames with amounts of transverse reinforcement within the ranges recommended in current design guidelines. The models considered represented idealized structures with initial periods of vibration ranging from 0.6 to 3 seconds and base shear strengths of approximately 15 and 30% of the total weight of the building.

5.2 Conclusions

On the basis of the experimental observations and their analyses, the following conclusions are made:

- 1) Displacement cycles at drift ratios not exceeding the drift ratio at yield do not affect the drift capacity of a reinforced concrete column.
- Column drift capacity was found to be sensitive to displacement history. For columns cycled beyond yield, it decreases as a function of the amplitude and number of cycles the column has experienced.
- 3) Column stiffness decreases with increasing number of cycles at drift ratios exceeding the drift ratio at yield. The reduction in stiffness exceeds 20% after transverse unit strains exceed 3%.
- 4) The drift limit can be determined by estimating the maximum transverse unit strain (ε_t) using the following expression given the number and amplitude of applied cycles:

$$\varepsilon_{t} = \frac{1}{d - d_{c}} \sum_{i=1}^{n} 2 \cdot \delta_{max \, i} \cdot \left(1 - \frac{\gamma_{r \, i}}{\gamma_{max \, i}} \right) \tag{4.5-1}$$

 $\delta_{max\ i}$: Increase in transverse deformation related to loading up to a drift ratio equal to $\gamma_{max\ i}$. It can be estimated on the basis of material and geometric properties of the column as shown in Sections 4.3 and 4.4.

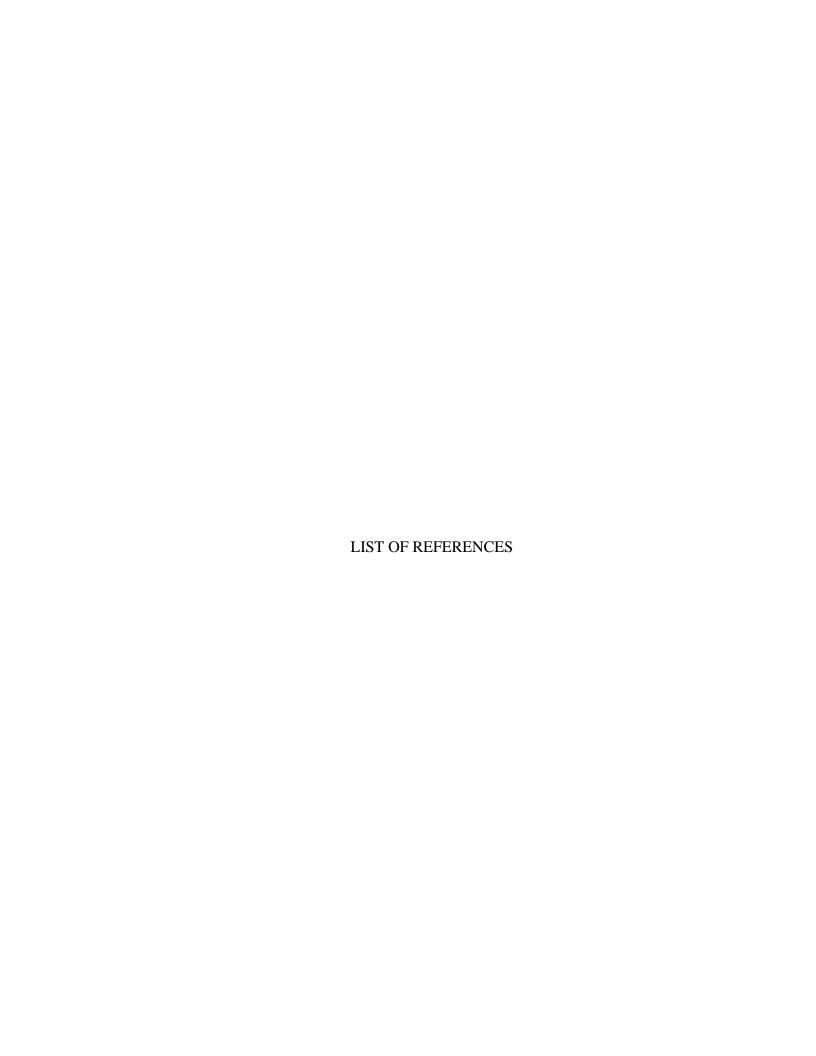
 $\gamma_{max i}$: Maximum drift ratio reached during cycle i.

 γ_{ri} : Decrease in drift ratio related to unloading from $\gamma_{max i}$. For the tests described here, assuming γ_{ri} equal to the drift ratio at yield led to conservative estimates of drift capacity.

n : Total number of cycles applied.

d: Effective depth

 $d_{\mathcal{C}}$: h - d, where h stands for cross-sectional depth.



LIST OF REFERENCES

- ACI Committee 318, 1999, "Building Code Requirements for Structural Concrete and Commentary," American Concrete Institute, Farmington Hills, Michigan 48333.
- Aktan, A. E., Karlson, B. I., and Sozen M. A., 1973, "Stress-Strain Relationships of Reinforcing Bars Subjected to Large Strain Reversal," *Structural Research Series No. 397*, University of Illinois at Urbana-Champaign, Civil Engineering Studies.
- Aoyama, H., 1993, "Design Philosophy for Shear in Earthquake Resistance in Japan," Earthquake Resistance of Reinforced Concrete Structures: A Volume Honoring Hiroyuki Aoyama, Ed. Tsueno Okada, November 25, pp. 140-151.
- Aschheim, M., 2000, "Towards Improved Models of Shear Strength Degradation in Reinforced Concrete Members," *Structural Engineering and Mechanics*, Vol. 9, No. 6, pp. 601-613.
- Blume, J. A., Newmark, N. M., and Corning, L. H., 1961, *Design of Multistory Reinforced Concrete Buildings for Earthquake Motions*, Portland Cement Association, Skokie, Illinois.
- Coulomb, C. A., 1773, "Essai sur une Application des Règles de Maximis & Minimis à quelques Problèmes de Statique Relatifs à l'Architecture," *Mémoires de Mathématique & de Physique, Présentés à l'Académie Royale des Sciences par divers savans, & lûs dans ses assemblées*, Paris, France, Vol. 7, pp. 343-382, (in French).
- Eberhard, M., and Parrish, M., 2000, "Reinforced Concrete Column Test Database," www.ce.washington.edu/~peera1.
- El-Bahy, A., Kunnath, S. K., Stone, W. C., and Taylor, A. W., 1999, "Cumulative Seismic Damage of Circular Bridge Columns: Benchmark and Low-Cycle Fatigue Tests," *ACI Structural Journal*, Vol. 96, No. 4, July-August, pp. 633-641.
- FEMA 273, 1997, "Guidelines for the Seismic Rehabilitation of Buildings," NEHRP, Federal Emergency Management Agency, Washington DC, October.
- Ingham, J. M., Liddell, D., and Davidson, B. J., 2001, "Influence of Loading History on the Response of a Reinforced Concrete Beam," *Bulletin of the New Zealand Society for Earthquake Engineering*, Vol. 34, No. 2, June, pp. 107-124.

- Iwasaki, T., Kawashima, K., Hasegawa, K., Koyama, T., Yoshida, T., 1987, "Effect of Number of Loading Cycles and Loading Velocity of Reinforced Concrete Bridge Piers," 19th Joint Meeting US-Japan Panel on Wind and Seismic Effects, UJNR, Tsukuba.
- Konwinski, C., 1996, "Shear Strength of reinforced Concrete Bridge Piers Subjected to Earthquake Loading," M.S. Thesis, School of Civil Engineering, Purdue University.
- Lepage, A., 1997, "A Method for Drift-Control in Earthquake-Resistant Design of R/C Building Structures," Ph.D. Thesis, Civil Engineering, University of Illinois, Urbana-Champaign.
- Mahin, S. A., and Bertero, V. V., 1981, "An Evaluation of Inelastic Seismic Desing Spectra," *Journal of the Structural Division*, ASCE, Vol. 107, ST9, pp. 1777-1795.
- Malone, B. J., 1999, "Shear Strength of Reinforced and Prestressed Concrete Beams With Lightweight Aggregate Concrete," Ph.D. Thesis, School of Civil Engineering, Purdue University.
- Matamoros, A. B., 1999, "A Study of Drift Limits for High-Strength Concrete Columns," Ph.D. Thesis, Civil Engineering, University of Illinois, Urbana-Champaign.
- Moehle, J. P., and Sozen, M. A., 1980, "Experiments to Study Earthquake Response of R/C Structures with Stiffness Interruptions," *Structural Research Series No. 482*, University of Illinois at Urbana-Champaign, Civil Engineering Studies.
- Moehle, J. P., Elwood, K. J., and Sezen, H., 2000, "Gravity Load Collapse of Building Frames During Earthquakes," M. Uzumeri Symposium, Special Publication, American Concrete Institute.
- Murakami, M., and Imai H., 1986, "A Study on Influence of Different Loading Histories on Failure Behavior of R/C Column Yielding in Flexure," *Transactions of the Japan Concrete Institute*, Vol. 8, pp. 367-380.
- Ohue, M., Morimoto, H., Fujii, S., and Morita, S., 1985, "The Behavior of R.C. Short Columns Failing in Splitting Bond Shear Under Dynamic Lateral Loading," *Transactions of the Japan Concrete Institute*, Vol. 7, pp. 293-300.
- Olesen, S. O., Sozen, M. A., and Siess, C. P., 1967, "Investigation of Prestressed Reinforced Concrete for Highway Bridges; Part IV: Strength in Shear of Beam with Web Reinforcement," University of Illinois Engineering Experimental Station, *Bulletin* 493, Vol. 64, No. 134, July.
- Ono, A., Shirai, N., Adachi, H., and Sakamaki, Y., 1989, "Elasto-Plastic Behavior of Reinforced Concrete Column With Fluctuating Axial Force," *Transactions of the Japan Concrete Institute*, Vol. 11, pp. 239-246.

- Park, R., 1989, "Evaluation of Ductility of Structures and Structural Assemblages from Laboratory Testing," *Bulletin of the New Zealand National Society for Earthquake Engineering*, Vol. 22, No. 3, September, pp. 155-166.
- Priestley, M. J. N., Verma, R., and Xiao, Y, 1994, "Seismic Shear Strength of Reinforced Concrete Columns," *Journal of Structural Engineering*, ASCE, Vol. 120, No. 8, August, pp. 2310-2329.
- Pujol, S., Sozen, M. A., Ramirez, J. A., 2000, "Transverse Reinforcement for Columns of RC frames to Resist Earthquakes," *Journal of Structural Engineering*, ASCE, Vol. 126, No. 4, April, pp. 461-466.
- Ramberg, W., and Osgood, W. R., 1943, "Description of Stress-Strain Curves by Three Parameters," National Advisory Committee of Aeronautics, *Technical Note 902*.
- Richart, F. E., 1927, "An Investigation of Web Stresses in Reinforced Concrete Beams," University of Illinois Engineering Experimental Station, *Bulletin No. 166*, June.
- Richart, F. E., Brandtzaeg, A., and Brown, R. L. 1929, "The Failure of Plain and Spirally Reinforced Concrete in Compression," University of Illinois Engineering Experimental Station, *Bulletin No. 190*, Vol. 26, No. 31, April.
- Saatcioglu, M., Ozcebe, G., 1989, "Response of Reinforced Concrete Columns to Simulated Seismic Loading," *ACI Structural Journal*, January-February, pp. 3-12.
- Sakai, Y., Hibi, J., Otani, S., and Aoyama, H., 1990, "Experimental Study on Flexural Behavior of Reinforced Concrete Columns Using High-Strength Concrete," *Transactions of the Japan Concrete Institute*, Vol. 12, pp. 323-330.
- Taylor, A. W., Stone, W. C., 1993, "A Summary of Cyclic Lateral Load Tests on Spiral Reinforced Concrete Columns," National Institute of Standards and Technology (NIST), Report NISTR 5285, United States Department of Commerce, Technology Administration.
- Taylor, A. W., Kuo, C., Wellenius, K., Chung, D., 1997, "A Summary of Cyclic Lateral Load Tests on Rectangular Reinforced Concrete Columns," National Institute of Standards and Technology (NIST), *Report NISTR 5984*, United States Department of Commerce, Technology Administration.
- Wight, J. K., and Sozen, M. A., 1973, "Shear Strength Decay in Reinforced Concrete Columns Subjected to Large Deflection Reversals," *Structural Research Series No. 403*, University of Illinois at Urbana-Champaign, Civil Engineering Studies.
- Xiao, Y., and Martirossyan A., 1998, "Seismic Performance of High Strength Concrete Columns," *Journal of Structural Engineering*, ASCE, Vol. 124, No. 3, pp. 241-251.
- Yamashiro, R., Siess, C. P., 1962, "Moment-Rotation Characteristics of Reinforced Concrete Members Subjected to Bending, Shear, and Axial Load," *Structural Research Series No. 260*, University of Illinois at Urbana-Champaign, Civil Engineering Studies.